Chapter 7

Experimental Section

This chapter outlines experimental methods, chemical syntheses and work not described in the main text. These include studies of 1,7-dichloroheptane/urea and 2,3,5,6-tetramethylpyrazinium-*N*-oxide, as well as the attempted synthesis of chiral deuterated 2,9-decanedione and an attempt at resolving guests in the crystal structure solution of a UIC crystal containing a mixture of 2,9-decanedione and 6-chlorohexyl acetate. In addition, the determination of the retraction rate of the ultrafast stress strain device (used in the kinetic studies of Chapter 4) is discussed. Finally, experimental details and synthetic procedures not introduced in Chapters 2-5 complete this chapter.

7.1 1,7-Dichloroheptane/urea

For crystals such as 2,9-decanedione/urea, the uniaxial optical symmetry allows the observation of optical rotation (Section 2.2.3). Unfortunately, the determination of absolute configuration of a UIC has not been possible via crystallographic methods. The guest 1,7-dichloro-4-heptanone was therefore designed[1] for the purpose of creating an optically uniaxial crystal with a heavy-atom containing guest that would allow for the determination of the absolute configuration, which could then be tied to the optical rotation of the crystal. Because the urea helix exhibits a reliable 11.0 Å repeat length for every helical turn, a guest whose length is 12.83 Å should span the length of about 7/6 helical lengths for a $6c_g' = 7c_h'$ commensurate structure. This behavior is exemplified in 2,7-octanedione/urea.[2] For this crystal, $c_g' = 12.85$ Å and the commensurate relationship is $6c_g' = 7c_h'$ with a 77.1 Å channel repeat and hexagonal metric symmetry. Although it

exhibits the stacked loop topology, each guest in the UIC of 1,6-dibromohexane spans 10.915 Å (at –60° C).[3] The large number of UICs of α,ω-dihaloalkanes[4-6] suggests that guests such as 1,7-dihaloalkanes should readily grow channel inclusion compounds with urea. In addition, the tendency for a guest ketone to act as a directing element in urea inclusion compounds has been established.[2,7] Thus, urea inclusion compounds of 1,7-dihalo-4-heptanone were sought. This study discusses the UIC containing the chloro-analogue: 1,7-dichloro-4-heptanone/urea.

Crystals of 1,7-dichloro-4-heptanone/urea were grown by Dr. Matthew Peterson, who also solved the crystal structure.[8] The data, collected at –70 °C, reveal a very nearly hexagonal unit cell. Peak integration produced the following cell constants, based on 17753 reflections (estimated errors, based on goodness of fit, are in parentheses):

a = 16.442 (2) Å	α = 90°
b = 10.9152 (14) Å	β = 119.698 (2)°
c = 16.426 (2) Å	γ = 90°.

From these data it is clear that the 77 Å channel axis repeat and the $6c_g' = 7c_h'$ topology it would imply are not present. Instead, the 10.9 Å (b) channel axis indicates a potential $c_g' = c_h'$ relationship in which the guest has shortened to accommodate the host repeat length. The structure solution and subsequent refinement indeed proved this to be the case. In the final structure, solved in $P2_1/c$, the guest molecules are coiled up to the extent that they fit into one channel repeat unit. This is illustrated in Figure 7.1a. Here, a cutaway view of the stacked loop channel is provided. In this crystal, the guest does not exhibit the all anti conformation observed in many other UICs. Instead, severe twisting across the C2-C3 (and analogous C6-C5) bond distorts the guest from the preferred

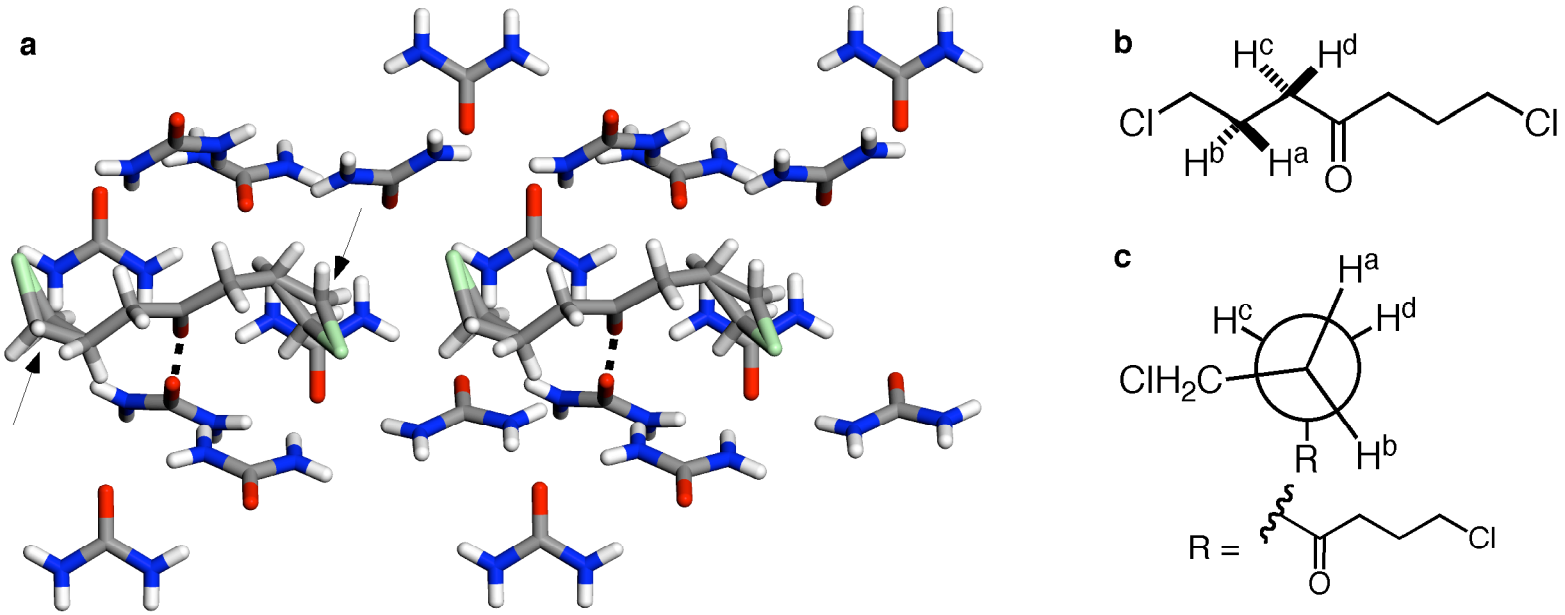

Figure 7.1 The crystal structure of 1,7-dichloro-4-heptanone/urea at –70° C. Space group: $P2_1/c$. (**a**) Cutaway channel view of this structure (along [001]) shows the guest to be appreciably coiled. By coiling, the guest is shortened to the extent that it fits into the 11 Å repeat of the urea helix. Disorder at C1 and C7 was refined with site occupancies of 68:32. (The arrows point to the minor carbon site.) (**b**) Schematic drawing of the guest and naming for Newman projection in **c**. The carbon atoms that comprise the guest chain are numbered left to right: C1, C2 (with H^a and H^b), C3 (with H^c and H^d), C4 (the acyl carbon), *etc*. (**c**) Newman projection, viewed along the C2-C3 bond, using the hydrogen naming scheme outlined in **b**. It is this bond that exhibits the greatest deviation from expected torsional angles. Instead of an antiperiplanar R-C3-C2-C1 (or R-C5-C6-C7) torsion, this angle is 83.7° (or 79.8°) for the majority population modeled at C1 and C7, respectively or 129.1° (or 112.7°) for the minority population modeled at these sites. Close inspection of the perspective provided in **a** reveals a close contact between guest ketone and urea carbonyl (see dotted lines). Here, the two carbonyls are very nearly oriented along a line with O-O distance 3.26 Å. This distance is only slightly greater than the van der Waals radius of two oxygen atoms (3.04 Å). Refer to text for a discussion. This structure was solved by Dr. Matthew Peterson (structure solution mp101).

conformation (Figure 7.1b–c). Towards the termini, C1 and C7 exhibit positional disorder and were refined using a two-site model. (The final refinement provided site occupancy factors of 68:32.)

Another important feature of this structure is the positioning of the guest ketone: as shown in Figure 7.1a, it is oriented head-to-head with a urea carbonyl. The four atoms that comprise C=O *vs*. O=C lie very nearly along a linear path (for the guest, C–O•••O (host) = 176.1°; for the host, C–O•••O(guest) = 176.3°); since the carbonyl dipoles oppose one another, this interaction appears unfavorable. Indeed, a survey of 80 crystals of small (less than 20 heavy atoms) organic molecules found that opposing carbonyl and nitrile dipoles were not favored.[9]

Although this crystal structure provides no short contacts between guest chlorines and hosts, the commensurate relationship observed in 1,7-dichloro-4-heptanone/urea suggests the presence of some favorable interaction between the two. Urea inclusion compounds of α,ω–dihaloalkanes have been studied extensively,[3-6,10] but diffraction due to the guest sublattice is not usually observed for UICs of α,ω–dichloroalkanes.[10-12] Although 1,7-dichloro-4-heptanone/urea forms a stoichiometric structure that diffracts strongly, its monoclinic symmetry makes it optically biaxial and discourages the measurement of optical rotation. For this reason, the guest 1,7-dichloroheptane appeared a reasonable candidate for crystal growth and structure solution.

The guest 1,7-dichloroheptane was obtained commercially (ChemSampCo), in 70% purity. Distillation of the crude mixture under reduced pressure (0.1 torr, T_{vapor} = 40–43 °C)[13] afforded the pure compound (by NMR). Slow cooling of methanol solutions of this guest and urea (0.30 and 2.0 M, respectively)[14] provided block or needle-like

crystals that appeared hexagonal in shape when viewed along their longest axis (see Figure 7.2a,b). From X-ray diffraction experiments (discussed below), this long aspect was found[15] to be parallel to the urea channel axis in a fashion similar to many UICs that grow as needles[7] (*c.f.* 2-decanone/urea). However, for many crystals, the crystal faces at which the channels terminate appear beveled when viewed from the side. This feature might be attributed to channel end surface roughening that results from longitudinal disorder of the guests during crystal growth or a non-zero interchannel guest offset ($\Delta g \neq 0$ Å).

An X-ray diffraction experiment with 1,7-dichloroheptane/urea, collected[16] at –140 °C, provides strong evidence for guest disorder. Unit cell refinement[17] with no symmetry constraints produced the following cell constants, based on 9410 reflections (errors based on goodness of fit in parentheses):

a = 8.1160 (4) Å	α = 89.990 (3)°
b = 14.0579 (7) Å	β = 90.007 (3)°
c = 10.9290 (5) Å	γ = 90.001 (3)°

V = 1246.94 (13) Å^3.

Within errors, this cell exhibits orthorhombic metric symmetry. Further refinement[18] of the same data with orthorhombic constraints produced the following cell constants (errors based on goodness of fit in parentheses):

a = 8.1162 (4) Å
b = 14.0585 (7) Å
c = 10.9292 (5) Å

V = 1247.04 (13) Å^3.

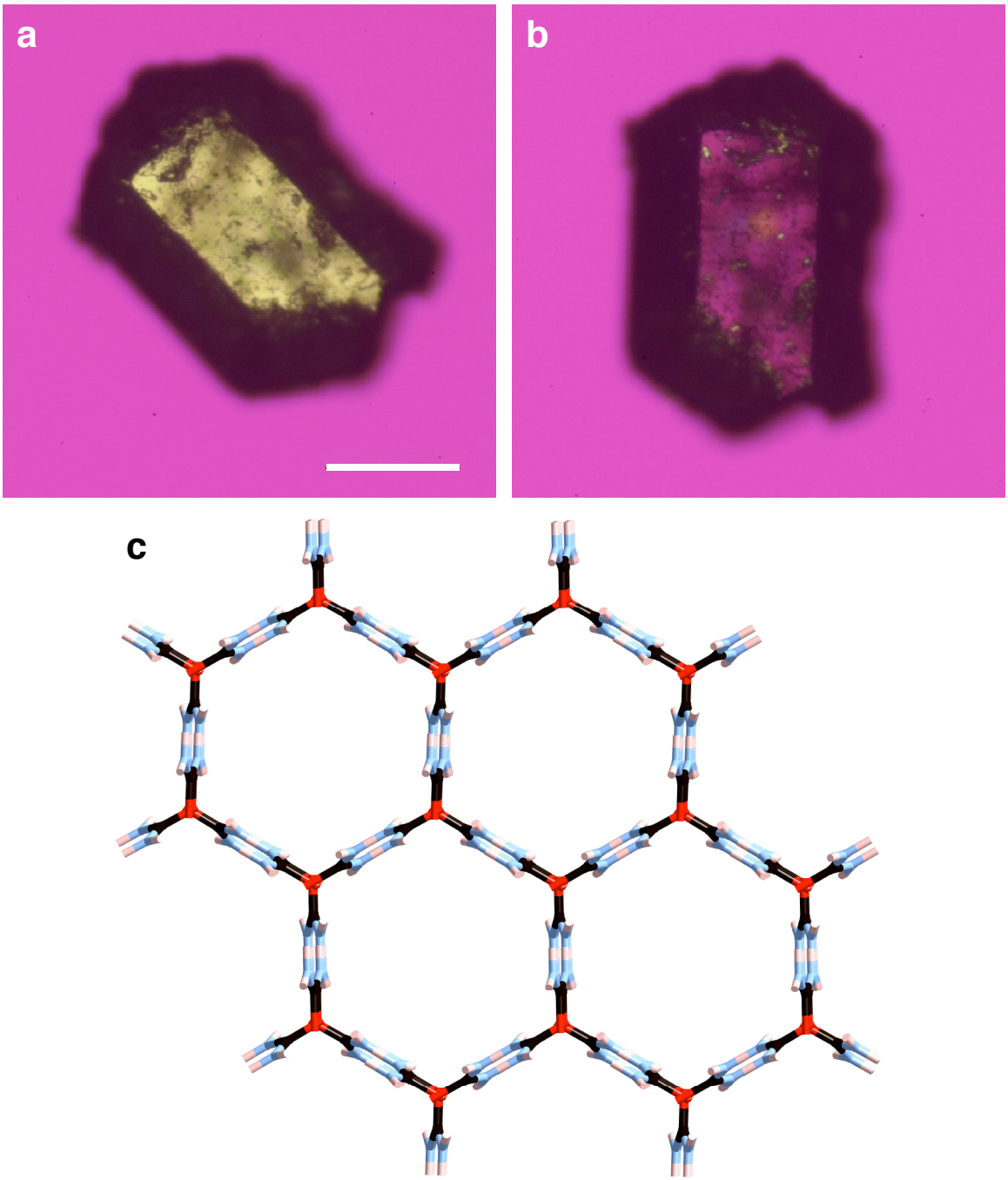

Figure 7.2 1,7-Dichloroheptane/urea. **(a,b)** Photomicrographs (taken between crossed polars and with λ plate) of the crystal used for X-ray data collection at –140° C. These photomicrographs were taken at two crystal orientations differing by 45°. Face indexing of this crystal shows the 10.9 Å channel axis, or [001], to run along the long dimension of this crystal. Beveling on this face of the crystal may be caused by longitudinal guest disorder or a non-zero interchannel guest offset, as discussed in the text. Scale bar = 0.25 mm (Nikon 4x). X-ray data set collection of the crystal shown in **a** and **b** was performed at –140° C and solved in $P2_1$. Although the guest sub-structure was not tractable, the host channel was well defined. **(c,d)** Plots of the crystal structure solution. In **c**, a group of channels is viewed along [001]. In **d**, one channel is viewed from an angle slightly off [001] so that the helical topology of the urea host can be observed. **(e)** ORTEP plot of the host structure, drawn at 50% probability. This plot was drawn using ORTEP-3 for Windows, Farrugia, L.J., *Journal of Applied Crystallography*, (1997), *30*, 565.

d

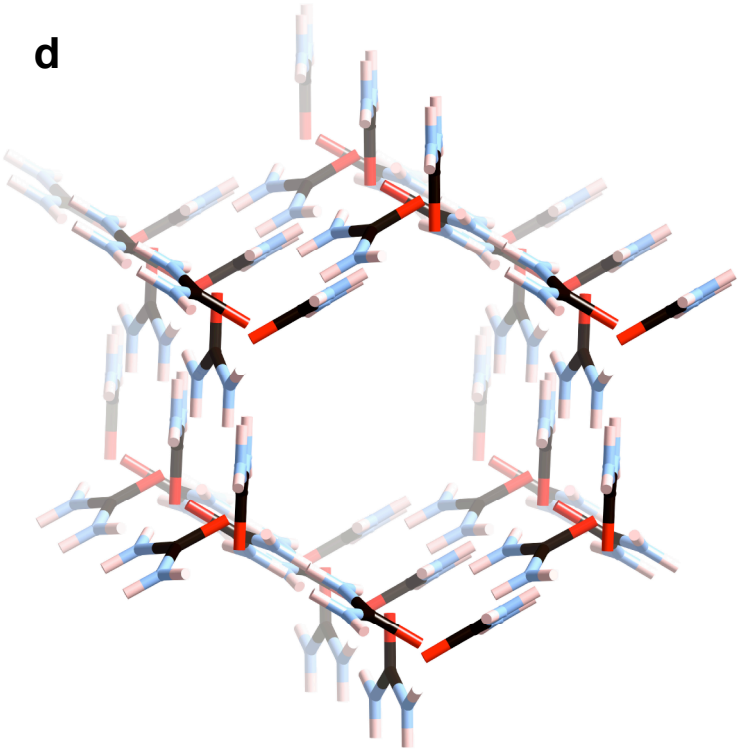

e

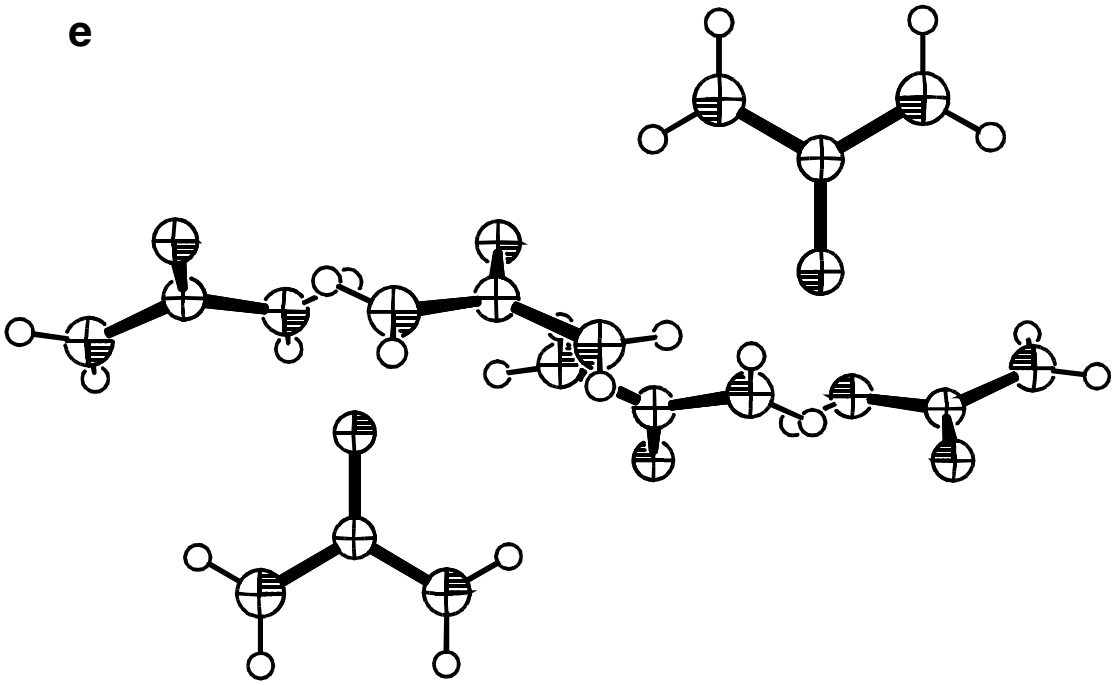

In an orthohexagonal cell, $b = a\sqrt{3}$. For a truly hexagonal lattice with b = 14.0585 Å, a = 8.1167 Å. Here, the a axis appears distorted by 0.0005 Å, a value comparable to the error limits of one standard deviation.) A survey of the reflections[19] provided many violations to lattice centering: for C-centering, there were 1983 of 4704 possible violations for which $I > 3\sigma$. For all reflections in this class, the mean $I/\sigma = 4.9$. (Other centering options produced stronger violations). However, a 2_1 axis along the [010] axis appeared plausible, with 0/15 violations with I > 3s (mean $I/\sigma = 0.3$). (A 2_1 axis along [100] produced 3/12 violations (with $I > 3\sigma$) with mean $I/\sigma = 8.6$, while neither a 2_1 nor a proper twofold rotation axis along the [001] (channel) axis are compatible with the guest and an 11 Å repeat.) This crystal was therefore solved with space symmetry $P2_1$ (b unique in the current cell setting).[20] In this solution, the urea host was located easily, but the guest was not. Unlike the structure of 1,7-dichloro-4-heptanone/urea, the urea channel is helical (see Figure 7.2d). Refinement[21] of the host molecules produced a maximum peak of 0.91 electrons/Å^3 in the residual electron density map. Although this peak was located in the interior of the channel, it was not possible to locate the remainder of the guest molecule, even with molecular insertion. In the end, the Fourier peaks that were observed within the channel were considered the result of a blurred distribution of electron density that is thought to represent longitudinal disorder of the guest. The problem of diffraction for incommensurate crystals such as alkanes and alkyl halides has been discussed by Harris and Thomas.[10] They show that the diffraction pattern from a UIC can be approximated by two distinct lattices. one of the host and the other for the guest, that interact with each other. The structure solution for the host in 1,7-dichloroheptane/urea unfortunately does not allow for the solution of the

guest; instead, the difficulty encountered in solving this structure suggests disorder in the guest substructure.

The diffraction of 1,7-dichloroheptane guest was also investigated using channel-axis X-ray oscillation photography. These experiments were performed by Mark Hollingsworth at the Université de Rennes, France. In the experiment, the crystal is mounted and carefully aligned so that it can be rotated about its channel axis (typically, by means of rotation about the goniometer ϕ axis). Depending on the crystal system, the range of rotation (typically 60 or 120°) is chosen to cover all symmetry equivalent Miller planes that are accessible with that mounting geometry. In the image obtained, c^* (the reciprocal c-axis) is represented along one direction of the image, while a^*b^* appears along the perpendicular. In the room-temperature oscillation image, the presence of discrete host reflections and diffraction rings (resulting from tetragonal urea created by crystal decomposition) are obvious (Figure 7.3a). On closer inspection, the presence of broad, diffuse bands can be discerned. These bands are important because they demonstrate coherent guest diffraction, which had not been observed previously.[12,22] Exciting as this discovery may be, these bands also provide important clues to the structural aspects of this UIC.

The use of a flat detector to record X-ray reflections makes the oscillation image appear "warped." Using a computer program[23] written by Philippe Rabiller (Université de Rennes), it is possible correct for the flat shape of the X-ray detector and "unwarp" oscillation images such as the one shown in Figure 7.3b. In this image, c^* is horizontal and a^*b^* is vertical. As with crystals such as 2-decanone/urea (Chapter 3), this image contains discrete spots, which are attributed to the host substructure, and diffuse bands,

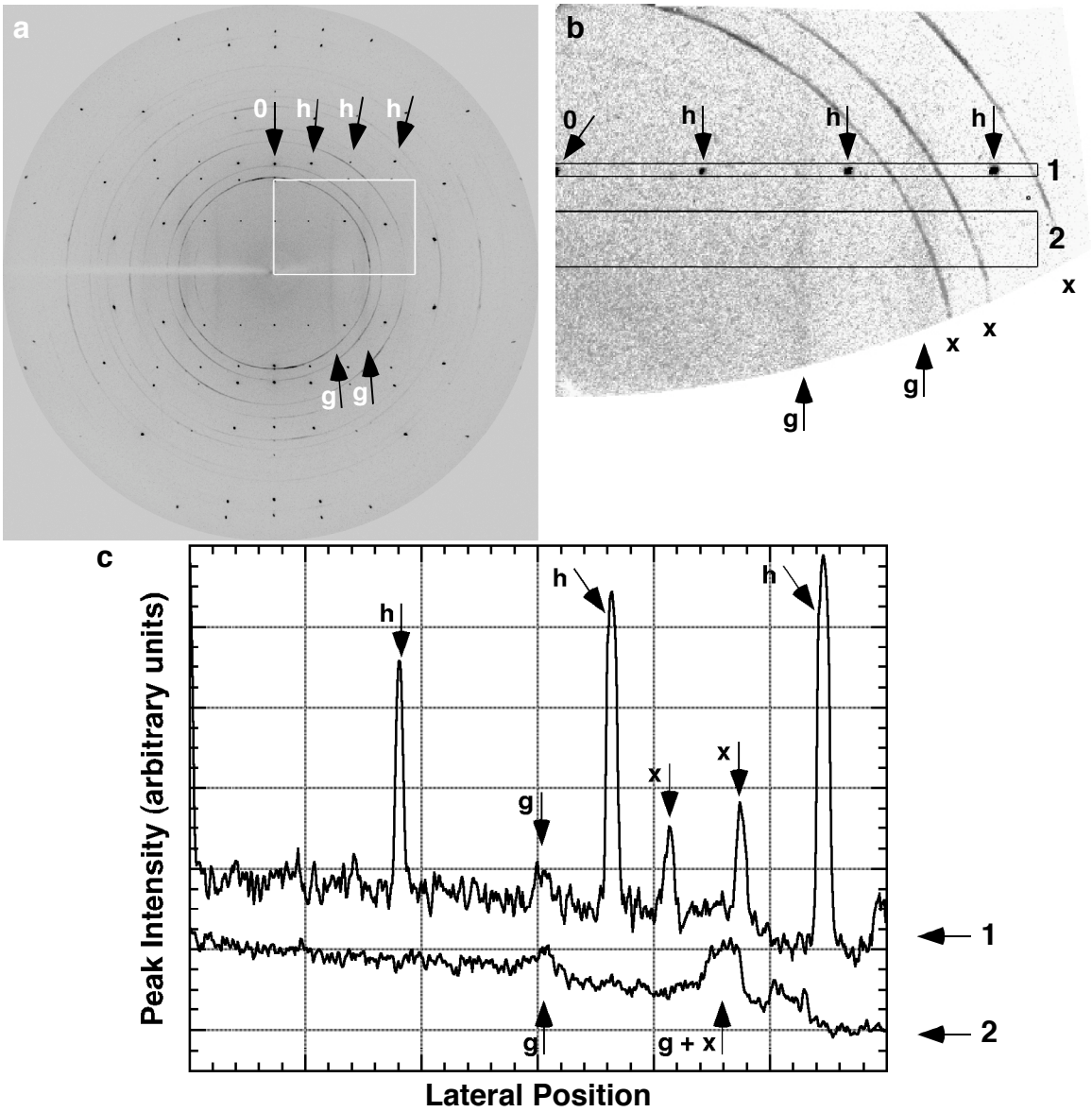

Figure 7.3 Channel-axis X-ray oscillation image of 1,7-dichloroheptane/urea, taken at 295 K. Here, the crystal was mounted so that the c* is horizontal. The flat detector used provides the apparent "warping" in these images. **(a)** The full oscillation image. Here, discrete spots from the host are visible with an 11 Å repeat length. These are denoted by h. Also observed are diffuse bands that run along the vertical. **(b)** A digitally "unwarped" image of the region outlined in **a**. In this image the diffuse bands are readily observable and are denoted by g. **(c)** Line profile plots of regions 1 and 2 (outlined by the boxes) in **b**. Region 1 (top profile) is 20 px tall and includes both host reflections and guest bands. (Some decomposition of the crystal resulted in diffraction rings from tetragonal urea. These are denoted by x in **a** and **b**). Region 2 (bottom profile) is 80 px tall and includes only the guest bands (and diffraction rings). In the images and line profiles, the first guest layer line is not observed, but the second and third are. The d-spacing for guest bands is 13.2 (1) Å.

which are attributed to the guest substructure. Since the diffuse bands run along a^*b^*, the guest is disordered along the *ab* plane, or perpendicular to the urea channel. Line profiles of peak intensity *vs*. position for two boxed regions in the unwarped image are provided in Figure 7.3c. Here, the disparity in peak intensity and sharpness between the "host" and "guest" layer lines is apparent. By comparing the spacing between the host layer lines (which exhibit 11.0 Å spacing) and guest layer lines, it is possible to estimate the repeat spacing for the guest layer lines. For the second guest layer line (the first is not visible), c_g = 13.2 (1) Å, a guest length consistent with that anticipated from simple molecular modeling. (Here, the error arises from uncertainty in the position of the reflection maxima for the guest layer lines.) Apparently, this guest does not become coiled to achieve the 11.0 Å repeat observed for 1,7-dichloro-4-heptanone/urea. It is also important to note that 13.2 Å is the ideal guest length for a commensurate relation of $5c_g' = 6c_h'$. For this relationship to hold, the sixth guest layer line and fifth host layer line should be coincident. Unfortunately, these high index layer lines were not observable. It is therefore not possible to discuss with certainty whether or not this crystal is commensurate.

The images in Figure 7.3 provide an additional detail: the band broadness of the guest layer lines increases with scattering angle. This can be observed in the unwarped oscillation image (Figure 7.3b). Unfortunately, diffraction intensity for the third guest layer line is superimposed upon the second diffraction ring from tetragonal urea (see x in Figure 7.3b) so it is not possible to quantify the width of this third layer line, even though the image suggests that this layer is broader and more diffuse than the second layer line. (The question of broadening at higher indices was addressed by creating plot profiles at

different vertical positions. Unfortunately, the overlap between this guest layer line and the diffraction ring is such that the intensity from the guest layer line became indistinguishable from noise in the diffraction image when a thinner line profile was measured. At locations too far from vertical center, the intensity of these bands decreases; too close to center, and the line profile no longer samples the unwarped image.) Such broadening of reflections at increased scattering angle has been attributed to the disruption of short-range crystalline order over long distances. Such *disorder of the second kind*[24] could occur in this crystal if guest spacing is well correlated, but only over relatively short distances.

Some understanding of the differences between UICs of 1,7-dichloroheptane and 1,7-dichloro-4-heptanone come from a study of their thermal stability. Using differential scanning calorimetry (DSC) it is possible to observe the thermal behavior of these crystals at various temperatures. Figure 7.4 provides plots of heat flow vs. temperature for both kinds of crystals. When 1,7-dichloroheptane/urea is warmed at 10 ºC min^{-1}, an endothermic event is observable at T_{onset} = 62.6 °C; upon cooling, an exotherm is observed at 40.7 °C (Figure 7.4a). The enthalpies of these transitions were calculated assuming a $5c_g' = 6c_h'$ structure; for the endothermic event, the enthalpy (ΔH) = 10.4 kcal $(mol\ guest)^{-1}$, while for the exothermic event, $\Delta H = -5.3$ kcal $(mol\ guest)^{-1}$. Because both species are in equilibrium at the phase transition, the free energy change, ΔG, is zero. Using the Gibbs equation, the phase transition entropy can therefore be calculated using the transition temperature and the transition enthalpy. For these transitions, ΔS = 31.0 and –16.7 cal $(mol\ guest)^{-1}$, respectively. It is unclear why the change in enthalpy (and entropy) observed for the cooling transition is so much less than that for the heating

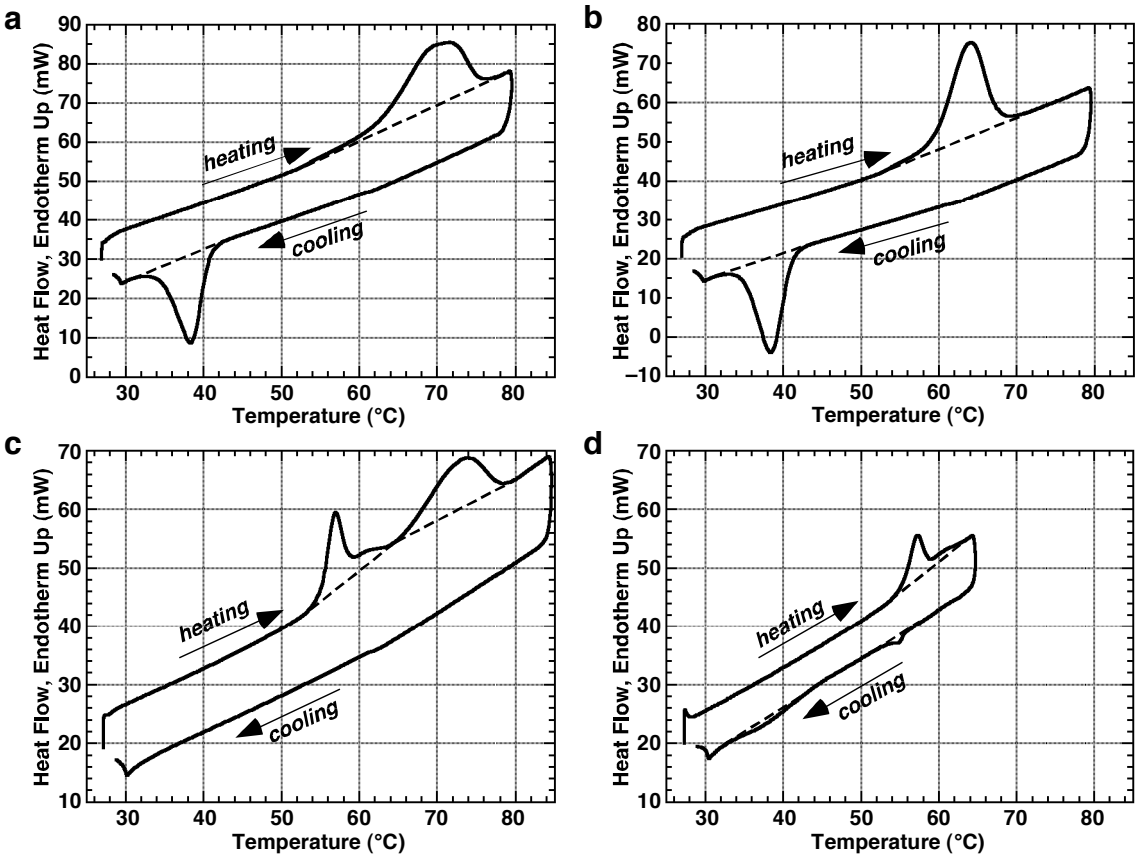

Figure 7.4 Differential scanning calorimetry (DSC) of UICs containing 1,7-dichloroheptane or 1,7-dichloro-4-heptanone. **(a-b)** DSC of 11.27 mg of lightly crushed 1,7-dichloroheptane/urea. (**a**) Upon heating (from room temperature) at 10 °C min^{-1}, an endothermic transition was observed with an onset temperature (T_{onset}) of 62.6 °C (69.7 °C peak) and transition enthalpy (ΔH) of 10.4 kcal (mole guest)$^{-1}$. (This enthalpy assumes a 13.2Å guest repeat length and $5c_g = 6c_h$ relationship.) When cooled at the same rate, the exothermic transition occurred at T_{onset} = 40.7 °C (38.4 °C peak) with ΔH = –5.3 kcal (mole guest)$^{-1}$. These transitions were again observable in a second experiment with the same sample (**b**); here, T_{onset} = 59.4 °C (64.1 °C peak) with ΔH = 10.1 kcal (mole guest)$^{-1}$ upon heating and T_{onset} = 41.1 °C (38.4 °C peak) with ΔH = –7.5 kcal (mole guest)$^{-1}$ upon cooling. **(c-d)** DSC of 1,7-dichloro-4-heptanone/urea. **(c)** The first sample of 1,7-dichloro-4-heptanone/urea contained 8.44 mg of lightly crushed crystal. Upon heating (from room temperature) at 10 °C min^{-1}, two distinct endothermic transitions are observed; the first has T_{onset} = 55.3 °C (57.0 °C peak) and ΔH = 4.0 kcal (mole guest)$^{-1}$. (This endotherm involves two events; see hump above 60 °C.) The second transition occurs at T_{onset} = 66.3 °C (73.3 °C peak) and ΔH = 6.3 kcal (mole guest)$^{-1}$. Upon cooling, no exotherm is observed for this crystal (the small exotherm near 62 °C is visible in DSCs of unrelated samples and is presumed an artifact). **(d)** A fresh sample containing 4.15 mg lightly crushed 1,7-dichloro-4-heptanone/urea. This sample was heated at 10 °C min^{-1} to a maximum temperature of 65 °C so that the large endothermic event at ~65–70 °C was not observed. In the heating curve, the pair of events observed in **c** occur, with T_{onset} = 55.4 °C (57.2 °C peak) and ΔH = 4.5 kcal (mole guest)$^{-1}$. Upon cooling, two small exotherms are observed. The first is fairly abrupt, T_{onset} = 55.7 °C (55.0 °C peak) and ΔH = –0.4 kcal (mole guest)$^{-1}$. The second exotherm appears very broad, with T_{onset} = 40.4 °C (37.4 °C peak) and ΔH = –0.2 kcal (mole guest)$^{-1}$.

transition; however, the reproducibility of these values suggests the discrepancy may not arise from measurement errors. Indeed, the second run (Figure 7.4b), performed on the same sample using the same temperature program, provides a reasonably similar DSC; here the endotherm appears narrower than in the first run. Although for the second run the temperature of the endothermic event decreases slightly (to 59.4 °C), the measured enthalpy (10.1 kcal (mol guest)$^{-1}$) is quite similar to the value measured for the initial run. (For this transition, ΔS = 30.4 cal (mol guest)$^{-1}$.) Upon cooling the second time, T_{onset} = 41.1 °C, ΔH = –7.5 kcal (mol guest)$^{-1}$ and ΔS = –23.9 cal (mol guest)$^{-1}$. The moderately consistent behavior observed for both DSC trials suggests that the endothermic transition is reversible and nondestructive. Although channel-axis oscillation images recorded at elevated temperatures reveal polycrystalline diffraction rings indicative of tetragonal urea,[11] the reversibility of this phase transition suggests that it does not involve decomplexation of 1,7-dichloroheptane/urea. Calorimetry experiments performed at low temperatures indicate no anomalous thermal behavior to –180 °C.[25]

For 1,7-dichloro-4-heptanone/urea, the DSC output (Figure 7.4c–d) appears somewhat different. Upon heating, the sample exhibits at least two endotherms. The first event occurs at T_{onset} = 55.3°C, while a broader endotherm occurs at T_{onset} = 66.3°C. A shoulder on the first event suggests another event, with a peak temperature of approximately 61 °C. There are no other thermal anomalies to over 100°C. In additional experiments performed using a fresh sample, the first thermal event (and shoulder) appeared to be reversible (see Figure 7.4d) as long as the temperature was not heated above 65 °C. However, it appears that the thermal event at T ~65° is irreversible; the absence of a corresponding event in the cooling curve of Figure 7.4c suggests that this

event involves a permanent change in the UIC, possibly decomplexation. In addition, the thermal event(s) in the heating curve of Figure 7.4d (T ~55° and ~61 °C) appear to be nondestructive. (A second run for this sample produced a very similar DSC.[26]) This assertion agrees well with the observation of no exothermic events in the cooling curve of Figure 7.4c: for this sample, an irreversible event (decomplexation) has apparently occurred.

7.2 Progress in the Synthesis of Chiral 2,9-decanedione

To date, 2,9-decanedione has been synthesized via the oxidation of 1,9-decadiyne with mercuric oxide.[7] Although facile and high yielding, the increasing cost of decadiyne starting material and the incompatibility of this method with the construction of a chiral deuterated product demanded an alternative synthetic strategy. (As deuterons are efficient neutron scatterers, the structure solution of a chiral deuterated analog of 2,9-decanedione in urea provides an attractive route for linking optical rotation and channel handedness, a correlation so far based on empirical evidence.[27]) The success of the acetoacetic ester synthesis of 2,10-undecanedione, a method pioneered in this laboratory by Terry Geiger, made this route attractive for the stereospecific synthesis of an enantiomer of 5,6-dideutero-2,9-decanedione as well. The acetoacetic ester synthesis, outlined in Figure 7.5a, consists of the nucleophilic substitution reaction between an α-ω-dibromoalkane and the anion of ethyl acetoacetate to produce a (bis)acetoacetic ester intermediate. Foregoing deliberate isolation, this diester is saponified in base (NaOH) and then decarboxylated in strong acid, respectively, to yield the diketone product.

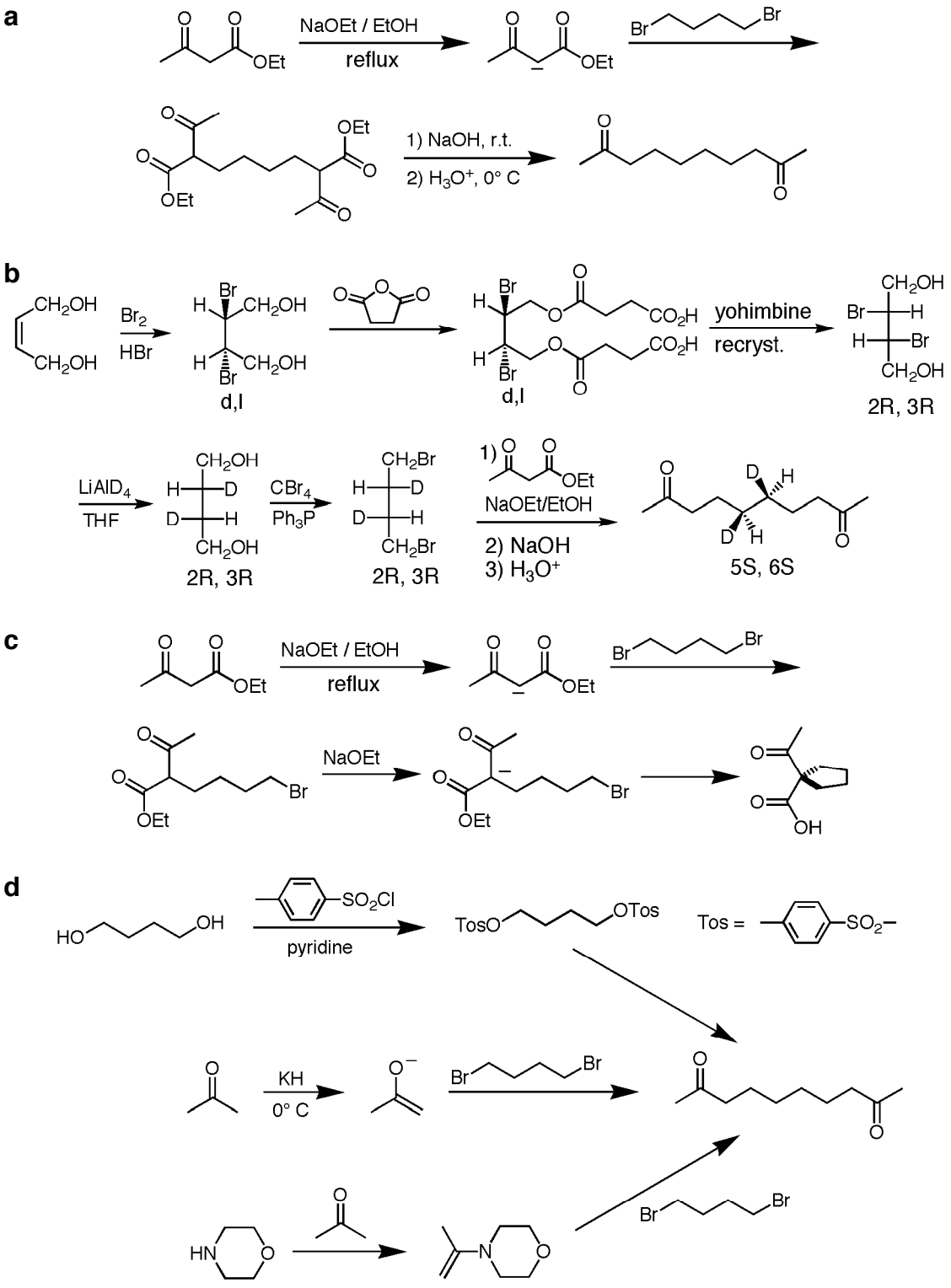

Figure 7.5 Synthetic schemes utilized in the synthesis of (5S,6S)-5,6-dideutero-2,9-decanedione. **(a)** Acetoacetic ester condensation. **(b)** The proposed synthetic scheme for the resolution of the chiral precursors and formation of the final product. **(c)** The side reaction proposed for the acetoacetic ester reaction. **(d)** Proposed alternatives to the scheme in **a**, including the introduction of better leaving groups and carbanion equivalents.

This acetoacetic ester route to 2,9-decanedione compliments the synthetic strategy developed by Mark Hollingsworth for the construction of a chiral deuterated analog (Figure 7.5b). In this strategy, the bromination of commercially available 2-butene-1,4-diol produces the dibrominated product, which is a racemate of (*R*,*R*) and (*S*,*S*) products. Enantiomeric purification of this intermediate has been demonstrated in the literature[28] and is performed as follows: The 1,4-diol is converted to the dihemisuccinate ester by condensation with succinic anhydride. This hemisuccinate is then crystallized in the presence of yohimbine, a chiral alkaloid isolated from the johimbe tree.[4] Following isolation of the yohimbine-(2*R*, 3*R*)-hemisuccinate adduct, deesterfication is performed by refluxing the enantiomerically purified product in ethanol with HCl, affording the (2*R*, 3*R*) diol and diethyl succinate, which is removed by distillation.

At this point, (2*R*, 3*R*)-(+)-2,3-dibromobutane-1,4-diol is reduced with $LiAlD_4$ to yield stereopure (2*R*, 3*R*)-(+)-2,3-dideuterobutane-1,4-diol. Substitution of the terminal alcohols under the action of carbon tetrabromide produces the precursor to the acetoacetic ester condensation, (2*R*, 3*R*)-(+)-1,4-dibromo-2,3-dideuterobutane.

Currently, practicality of the much of the preceding synthesis remains to be explored. In preliminary trials, performed by Alia Clark, Jeremy Rush, and Terry Geiger[22] the acetoacetic ester condensation of 1,4-dibromobutane has proven unsuccessful. Here, the condensation of acetoacetic ester anion with unlabelled dibromide produces the cyclic byproduct (Figure 7.5c) in appreciable yield,[22,29] even when performed using a large excess of acetoacetic anion. However, alternate routes from 1,4-dibromobutane to 2,9-decanedione have been examined. These are discussed below.

In considering the problem of alkylating 1,4-dibromobutane, the solution can be approached from two directions. First, the reactivity of the leaving group can be improved. For instance, for the scheme provided in Figure 7.5d, the alkyl bromide has been replaced by an alkyl tosylate, which is approximately 2600 times more reactive than a primary bromide in model nucleophilic substitution reactions.[30] This precursor was produced in 57% yield by addition of 1,4-butanediol to a solution of tosyl chloride in an excess of pyridine and methylene chloride solvent.[31] However, by improving leaving group affinity, one is not addressing directly the issue of intramolecular ring closure by the monosubstituted intermediate in Figure 7.5c. If ring closure is faster than intermolecular substitution, then improving the leaving group affinity may only improve the yield of the undesired product. (It may be argued, however, that the larger tosyl group could actually inhibit ring closure.) Clearly, the potential for ring closure must be eliminated entirely for this synthetic strategy to be fruitful.

One promising route to the alkylation of the dibromobutane adduct involves usage of other carbanion equivalents such as enolates or enamines (Figure 7.5d). For example, the substitution of bromines of 1,4-dibromobutane with acetone enolate should provide the desired product, with little anticipated capacity for ring closure or other side reactions. Fortunately, acetone enolate is known in the literature: the formation of the enolate in high yield from acetone and potassium hydride in THF solvent has been demonstrated.[32] The addition of dibromobutane to a solution of the anion at dry ice-acetone temperature should yield the desired 2,9-decanedione. However, the attempt of this synthesis produced only starting materials (as indicated by TLC and NMR of the reaction mixture).[33] This reaction was conducted only once; the relative

straightforwardness of this procedure warrants further exploration. There are several possible sources of error in the experiment. In this trial, the acetone had been distilled from Drierite desiccant and was considered quite dry. However, the dibromobutane (Acros 99%) was not itself purified. Certainly, the presence of small amounts of water (or other protic impurities) in this starting material will suppress the formation of acetone anion. Another complication lies in the potassium hydride; the history of this material was unknown. (It was obtained from the laboratory of Prof. Keith Buszek.) As supplied (from Aldrich), this material consisted of a slurry in mineral oil; perhaps new material or some other form of delivery would be more effective. Finally, the modest cost of acetone and potassium hydride dictates that an extremely large excess of both reagents be used, perhaps without the introduction of additional solvents.

Fortunately, a variety of acetone enolate equivalents are possible. Because of their well-documented chemistry[34-37] and relative ease of use,[38] enamines were considered a most favorable possibility. In Figure 7.5d, the construction of the acetone enamine from morpholine[36] produces the desired anion equivalent; subsequent alkylation by dibromobutane should produce 2,9-decanedione product in high yield. The simplicity perceived for this sort of chemistry allowed for its introduction into an undergraduate research-based course.[39] Unfortunately, despite repeated attempts at producing the enamine, no appreciable product was formed. These attempts included the use of dehydrating agents such as $TiCl_4$[40-42] and azeotropic removal of the water produced in the condensation of morpholine and acetone by toluene. The problems probably encountered with this reaction are similar to those anticipated for the potassium enolate formation: impure (wet) solvents and/or starting materials. Although it deserves further

consideration, this strategy may not be advantageous, as the reaction of simple enamines with weakly activated alkyl halides is not considered especially favorable.[35] (Of course, the utilization of a better leaving group, *e.g.,* tosylate, or the use of enamines based on pyrrolidine[35] may improve the feasibility of this pathway.) In any event, both the condensation of acetone enolate and the reaction of acetone enamine with 1,4-dibromobutane (or a more reactive equivalent) provide potential alternatives to the acetoacetic ester condensation and the synthesis of a chiral decanedione guest.

7.3 Attempted Crystal Structure Solution of a UIC Containing a Mixture of 2,9-Decanedione and 6-Chlorohexylacetate

The optically anomalous behavior fostered by the incorporation of 2-decanone into UICs of 2,9-decanedione suggests that this guest is included in a non-random fashion, as described in Section 2.2.3. For mixed crystals, the preferential ordering and/or incorporation of guests at particular growth sites may be probed by X-ray crystallography on mixed crystals of monoketone and diketone. However, the guests 2,9-decanedione and 2-decanone differ by only six electrons, so these guests would be difficult to distinguish in an X-ray diffraction experiment.

For the decanedione series, it was thought that a heavy-atom mimic of one of the guests could provide a means by which the two constituents could be differentiated in the X-ray data. For some time, heavy-atom mimics have been used extensively in areas such as protein crystallography and in other cases where a small portion of an X-ray visible "label" was instrumental in determining the phases of the diffraction data.[43] In the current case, an ideal 2-decanone "mimic" would contain a heavy element with a high X-

ray scattering factor that could be distinguished easily from other light scatterers (containing only carbon, hydrogen, oxygen and nitrogen), would be straightforward and inexpensive to produce, and, most critically, would exhibit characteristics of incorporation similar to 2-decanone. A potential candidate was found with the monoester 6-chlorohexyl acetate. This guest is easily prepared via condensation of 6-chloro-1-hexanol and acetic anhydride.[44] If incorporated into a UIC crystal containing mostly 2,9-decanedione, the presence of a chlorine scattering element can help differentiate this guest from the ubiquitous diketone. Molecular modeling (at the AM1 level of theory[45]) by Mark Hollingsworth indicates comparable gas-phase molecular lengths of 2-decanone (11.35 Å, C01 to C10) and 6-chlorohexyl acetate (11.24 Å, C01 to Cl). This can be attributed to the similarity in the effective volumes of aliphatic alkyl chlorides (19.3 $Å^3$) and methyl groups (22.7 $Å^3$).[46] Since 2,9-decanedione and 2-decanone are naturally longer than necessitated by the $3c_g' = 4c_h'$ commensurate repeat, the slightly smaller chlorine atom might encourage improved characteristics of incorporation.

For this experiment, crystals were grown in a methanol solution of 1.9 M urea containing a 75:25 ratio of 2,9-decanedione and 6-chlorohexylacetate.[47] As demonstrated by the crystal in Figure 7.6, the specimens collected exhibit very weak interference colors when viewed under the polarizing microscope. This crystal is viewed along the channel axis, which is the optic axis in pure 2,9-decanedione/urea (Section 3.1.3). By breaking the uniaxial symmetry of 2,9-decanedione/urea, the incorporation of a guest impurity such as 6-chlorohexyl acetate should make the crystal appear birefringent when viewed along this direction. Although the guest stoichiometry was not determined for this crystal, NMR analysis of another crystal from the same batch (with 10 s recycle delays)

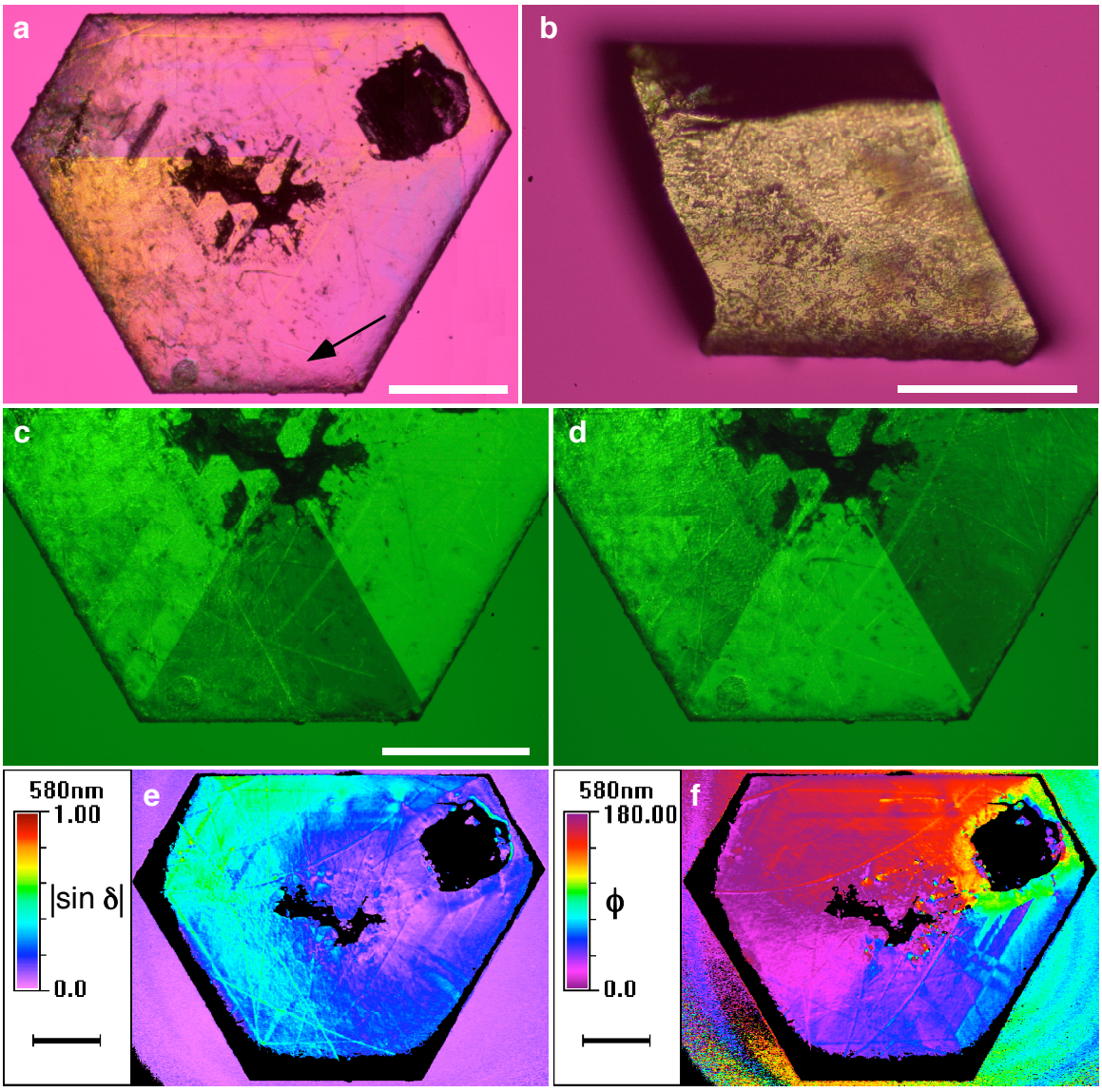

Figure 7.6 A UIC grown from a solution containing a 75:25 mixture of 2,9-decanedione and 6-chlorohexyl acetate. **(a)** Composite image (from three photomicrographs), taken between crossed polars and with λ plate, demonstrates the weak interference colors observed in this crystal when viewed along the channel axis. (The yellow appearance of the sector at left results from merging multiple images and not from guest zoning.) Before these photomicrographs were collected, the crystal was polished on lens paper using a 1:1 solution of methanol and ethanol; note the visible scratch marks. This crystal is 0.32 mm thick. Scale bar = 1.0 mm (Nikon 1.3x). **(b)** Crystal fragment for X-ray diffraction, in the same orientation as **a** (growth face at bottom). Mark Hollingsworth cleaved this fragment from the lower right section of the crystal in **a**, near the arrow. Scale bar = 0.20 mm (Nikon 10x). **(c,d)** Photomicrographs taken with uncrossed polars and green interference filter. Scale bar = 1.0 mm (Nikon 1.3x). **(c)** Analyzer at –10°. Here, dextrorotatory regions appear darker than in **d**. **(d)** Analyzer at +10°. Here, levorotatory regions appear darker than in **c**. From these, the sector used for diffraction is dextrorotatory. **(e,f)** Metripol images of the crystal, taken prior to cleavage. Scale bar = 0.69 mm (Metripol 1.3x). **(e)** Phase retardation (|sin δ|) image illustrates the weak birefringence observed in this crystal. The differences in retardation do not appear to adhere to a pattern rationalized as guest zoning. Scratches from polishing are also readily visible in this image. **(f)** Orientation image. Here, the crystal exhibits apparent growth sectoring; however, the extremely low birefringence of this crystal makes orientation assignments uncertain. Continued on next page.

(g,h) X-ray reflection intensities in (0 0 *l*) for the UIC crystal containing a mixture of ~92:8 2,9-decanedione:6-chlorohexyl acetate. **(g)** For space group $P3_112$, the limiting condition for reflection is $l = 3n$; these reflections are tabulated with their observed structure factor, multiplied by a factor of ten ($10F_o$), standard deviation in F_o ($\sigma(F_o)$), and average values of $10F_o$ (at bottom). **(h)** Twenty five observed reflections that do not satisfy the limiting condition ($l \neq 3n$). As discussed in the text, these intensities are appreciably lower than the allowed reflections, **(g)**.

g Reflections satisfying (00*l*), *l* = 3n

h	k	l	$10F_o$	$10\sigma(F_o)$
0	0	–33	93.86	3.76)
0	**0**	**–30**	**9.21**	**0.74**
0	0	–27	118.6	4.58
0	0	–27	120.2	4.59
0	0	–24	274.5	10.13
0	0	–24	276.5	10.10
0	0	–21	64.91	2.58
0	0	–21	66.00	2.60
0	0	–18	83.31	3.23
0	0	–18	85.85	3.24
0	0	–15	20.54	0.94
0	0	–15	21.14	0.94
0	0	–12	37.03	1.49
0	0	–12	37.34	1.50
0	0	–9	320.9	12.02
0	0	–9	345.1	11.97
0	0	–6	615.3	21.13
0	0	–6	621.3	22.87
0	0	–6	683.3	23.05
0	0	–3	54.25	2.02
		Mean	**198**	
		σ	**217**	

h Reflections violating (00*l*), *l* ≠ 3n

h	k	l	$10F_o$	$10\sigma(F_o)$
0	0	–32	0.52	0.41)
0	0	–31	0.21	0.36
0	0	–29	0.39	0.38
0	**0**	**–28**	**3.49**	**0.51**
0	0	–26	0.57	0.35
0	0	–23	0.10	0.25
0	0	–23	0.11	0.30
0	**0**	**–22**	**1.25**	**0.33**
0	**0**	**–22**	**1.88**	**0.31**
0	0	–20	0.20	0.24
0	**0**	**–19**	**1.13**	**0.28**
0	**0**	**–19**	**3.28**	**0.46**
0	0	–17	0.06	0.22
0	0	–17	0.39	0.22
0	0	–16	0.16	0.18
0	0	–16	0.22	0.23
0	0	–14	0.26	0.21
0	0	–13	0.12	0.17
0	0	–13	0.40	0.22
0	**0**	**–7**	**0.54**	**0.12**
0	0	–5	0.09	0.06
0	0	–5	0.17	0.07
0	**0**	**–5**	**0.30**	**0.06**
0	0	–4	0.04	0.04
0	0	–4	0.10	0.05
		Mean	**0.64**	
		σ	**0.93**	

(i,j) A comparison of bond distances and angles between the UIC crystal containing ~92:8 2,9-decanedione:6-chlorohexyl acetate ("mixed crystal") and 2,9-decanedione/urea ("2,9"). (Data for 2,9-decanedione from Brown, *et al*, *Science*, *273*, 1355 (1996)). **(i)** Here, bond types are classified according to their environment (i.e., guest ketone C=O vs. urea C=O, etc.). The largest discrepancy in bond lengths is with the guest alkyl chain: values for the mixed crystal (at –140° C) are, on the average, 2.8% longer than for the pure crystal (at room temperature). This discrepancy is also observed in the bond angles for the guest chain **(j)**: angles in the mixed crystals are some 4° smaller than for the pure crystal. These effects are indicative of reduced libration of the methylene chain at the low temperature used for the mixed crystal. In the room temperature structure, this libration serves to shorten the apparent bond length and increase the observed bond angles. The other bond lengths and angles are similar to 1% or, in most cases, much less.

i

Environment	Bond	Mixed crystal: bond distance, avg. (σ), Å	2,9/Urea: bond distance, avg. (σ), Å
Urea	C=O	1.261 (5)	1.259 (8)
	C–N	1.338 (3)	1.330 (7)
Guest Ketone	C=O	1.201*	1.204*
Guest Chain	C01–C02	1.453*	1.404*
	C02–C03	1.490*	1.456*
	C03 → C05	1.46 (2)	1.42 (2)

**There is only one of this bond type in the asymmetric unit*

j

Environment	Bond	Mixed crystal: bond angle, avg. (σ), deg.	2,9/Urea: bond angle, avg. (σ), deg.
Urea	N–C–N	118.0 (1.0)	118 (2)
	O–C–N	121.0 (5)	121.1 (7)
Guest Ketone	O-C-C	121.6 (8)	120.1 (1.3)
Guest Chain	C-C-C	118.4 (1.2)	123 (3)

indicated a relative diketone:monoester ratio of 12:1, or approximately 8% monoester incorporation.[48] Apparently, the monoester guest was not incorporated in large amounts so that optical anisotropy was induced only to a small degree; this guest does not appear to mimic the incorporation of 2-decanone into UICs containing mostly 2,9-decanedione adequately.

The insufficient incorporation of 6-chlorohexyl acetate could arise from the shorter length of this guest. A logical test of this hypothesis involves the substitution of bromine for chlorine on the monoketone mimic to yield 6-bromohexyl acetate. For the bromine atom, the effective volume is 23.9 $Å^3$, vs. 22.7 $Å^3$ for the methyl group.[46] This guest was prepared in a fashion similar to the chlorinated guest using the condensation of 6-bromo-1-hexanol and acetic anhydride.[49] Unfortunately, the brominated monoketone was not readily incorporated either: for crystals grown from a methanol solution of 1.7M urea and a 5:1 ratio of 2,9-decanedione and 6-bromohexyl acetate, NMR analysis indicated only trace amounts of the brominated monoester.[50] As with the chlorinated mimic, crystals containing mixtures of this guest and 2,9-decanedione were very weakly birefringent when viewed through their plate faces. The extremely small birefringence exhibited by these samples again suggests small amounts of incorporation, and no further analysis of such crystals was performed.

Regardless of the extent of monoester incorporation, an X-ray diffraction experiment was performed on a single crystal fragment cleaved from the crystal containing 6-chlorohexyl acetate. Figure 7.6e presents a phase retardation map of the crystal prior to dissection. In the upper left-hand portions of the crystal, $|\sin \delta|$ approaches a maximum of about 0.5. The sector from which the XRD fragment was

cleaved for diffraction produces values of |sin δ| from 0.25 to 0.35 units (Figure 7.6b). Although this crystal is clearly biaxial, the weak phase retardation makes accurate measurement of the retardation difficult.

Diffraction data for the fragment in Figure 7.6b was collected at –40 °C. Although a complete hemisphere was collected ($2.8 \leq 2\theta \leq 57.6°$, to 0.74 Å resolution), the Laue symmetry appears trigonal. Initial integration of 17419 reflections (15181 with intensity, I, > 3σ) and cell refinement with no symmetry constraints produced a unit cell with dimensions[51] (and standard deviations):

a = 8.128 (8) Å	α = 90.01 (3)°
b = 8.132 (10) Å	β = 89.99 (3)°
c = 43.91 (6) Å	γ = 119.98 (3)°

V = 2514 (9) Å^3.

Within the error of the refined lattice parameters, this cell is metrically trigonal. A second unit cell refinement of 11247 reflections (9722 with I > 3σ), with trigonal symmetry constraints, produced the following unit cell dimensions:[52]

a = 8.1364 (4) Å
b = 8.1364 (4) Å
c = 43.9285 (19) Å

V = 2518.5 (3) Å^3.

For this cell, strong systematic absence violations (mean I/σ > 20) were noted[53] for lattice centering as well as for 6_1 (or 6_5, mean I/σ = 14.2) and 6_3 (mean I/σ = 21.2) screw translations. For the 3_1 (or 3_2) screw axis, 33 violations were observed (for 5 of these, I > 3σ); for both axes, the violations' mean intensity = 0.5 and mean I/σ = 2.5. Although this mixed crystal should exhibit less symmetry than 2,9-decanedione/urea, the

space group $P3_112$ (#151) was selected as a starting point for this structure solution. The enantiomorphous $P3_212$ (#152) is also an option, but was not distinguishable[54] based on a comparison of equivalent reflections by the method of Flack (discussed below), so the original $P3_112$ solution was used.[55] For $P3_112$, an empirical absorbance correction yields R(int) = 0.032.

The structure solution produced a structure similar to that for 2,9-decanedione/urea (Section 1.1.2). Here, the $3c_g' = 4c_h'$ commensurate relationship is observed and, within the unit cell, three guests are related to one another by a threefold screw axis (in this case, right-handed) along the channel (*c*) axis. This structure refined quite nicely in $P3_112$: for the isotropic model,[56] the final cycle of full-matrix least-squares refinement was based on 11008 reflections (3822 unique) and 89 variable parameters and converged (mean shift/σ = 0.011 Å and max shift = 0.001Å for C01) with unweighted and weighted agreement factors for all data of:

R1 = $\Sigma\{|Fo| - |Fc|\}/\Sigma|Fo| = 0.1081$
wR2 = $\{\Sigma w(Fo^2 - Fc^2)^2/\Sigma[w(Fo^2)]^2\}^{1/2} = 0.3447$
where
$w = 1/(\sigma^2(Fo^2) + (aP)^2 + bP$
and
$P = [2(Fc^2) + \max(Fo^2, 0)]/3$
and a = 0.1, b = 0.

The goodness of fit (GooF) was 3.020 for all data and the extinction parameter (EXTI) refined to 0.031. The maximum and minimum peaks on the final difference Fourier map corresponded to 0.81 and –0.59 e/Å^3, respectively, none of which were located appropriately for a terminal chlorine. The Flack (x) parameter, which provides an estimation of the enantiomeric form of a structure solution, ideally ranges from 0 (for the

correct enantiomorph) to +1 (for the incorrect assignment).[55] For this model x = –0.6087 (2.5886). To test the possibility that the handedness of this structure was incorrect, the data was solved for the enantiomorphous $P3_212$ space group. For this solution,[57] x = 1.5224 (2.5903). The large errors in the Flack parameter do not allow one to make an assignment of absolute configuration, so the initial assignment of $P3_112$ was chosen arbitrarily. It is therefore not possible to correlate the absolute configuration of this fragment with its dextrorotatory[58] optical rotation.

For anisotropic refinement (of all non-hydrogen atoms) in $P3_112$, the final cycle of full-matrix least-squares refinement[59] was based on 3822 unique reflections and 201 variable parameters and converged (mean shift/σ = 0.000 Å and max shift = 0.000Å for O40) with unweighted and weighted agreement factors for all data of:

R1 = $\Sigma\{|Fo| - |Fc|\}/\Sigma|Fo| = 0.0499$
wR2 = $\{\Sigma w(Fo^2 - Fc^2)^2/\Sigma[w(Fo^2)]^2\}^{1/2} = 0.1610$
where
$w = 1/(\sigma^2(Fo^2) + (aP)^2 + bP$
and
$P = [2(Fc^2) + \max(Fo^2, 0)]/3$
and a = 0.1, b = 0.

For this refinement, the goodness of fit (GooF) was 1.374 for all data and the extinction parameter (EXTI) refined to 0.041. The maximum and minimum peaks in the final difference Fourier map corresponded to 0.31 and –0.24 e/Å^3, respectively. Neither of these were located in a position appropriate for a terminal chlorine atom. The absence of strong residual electron density in locations around the guest (prior to and following hydrogen atom insertion) underscores the difficulty in identifying the chlorinated guest at such low concentrations.

Another attempt to model 6-chlorohexyl acetate guest was conducted using space group $P3_1$ (#144). For this crystal, it is possible that the symmetry is less than $P3_112$ or $P3_212$, but that the threefold screw (which is favored by the host-guest hydrogen bond network) is retained. For the $P3_1$ solution,[60] ureas and 2,9-decanedione guest were easily identified. Using the coordinates of this guest, a second guest, 1,8-dichlorooctane, was created to model 6-chlorohexyl acetate in either of its possible orientations along the long axis of the channel. The occupancy of this second guest was refined[61] against the occupancy of 2,9-decanedione so that the sum of their populations equaled one. This refinement, performed without hydrogens and with isotropic thermal parameters, was not stable: the guest backbone fell apart regardless of modifications made to the input file. No further attempts to locate the second guest were performed.

To investigate the degree of symmetry reduction observed in the diffraction data, an analysis of the systematic extinctions for the 3_1 screw was performed. If the incorporation of 6-chlorohexyl acetate into sites normally occupied by 2,9-decanedione reduces the threefold symmetry along the channel, this might become apparent as distinct systematic absence violations for that symmetry element. For a threefold screw translation along [001], the limiting condition for reflection is,[62]

$$l = 3n \text{ for } (0\ 0\ l).$$

In this regard, reflections such as (0 0 2) and (0 0 7) are violations of this symmetry element, but (0 0 3) and (0 0 6) are not. The intensities of reflection violations may be useful in identifying the extent to which the incorporation of minor guest destroys the 3_1 screw symmetry element.

Data for reflections observed in (0 0 *l*) are tabulated in Figure 7.6g–h. Here, the observed structure factors (F_o) have been multiplied by a factor of ten ($10F_o$). In total, there are 45 reflections in class (0 0 *l*), of which 25 are systematic absence violations, with $10F_o > 0$ (mean $10F_o = 0.64$). Of these 25 violations, seven satisfy $10F_o > 3\sigma(10F_o)$; their average intensity is 2.2 and the most intense reflection, (0 0 $\overline{28}$), is 3.49 (0.51). (Here, σ represents one standard deviation in the determination of a given reflection intensity, as estimated by the SAINT integration software.[63]) By comparison, for the twenty *allowed* reflections in (0 0 *l*), the average intensity is 198 (217), with the intensities ranging from 9.21 to 683. The difficulty of accurately measuring a quantity that is less than 3σ has been addressed;[64] the eighteen reflection violations that do not meet this threshold are therefore considered indeterminate and are discarded from further analysis. The seven reflection violations that do meet this criterion are presented in bold in Figure 7.6h. For these, the intensities range from 0.30 to 3.49. In comparison to the structure factors of the allowed reflections, the seven reflection violations are extremely weak and are therefore considered unreliable. Although the incorporation of 6-chlorohexyl acetate guest should lower the symmetry of 2,9-decanedione, its effect is not readily observed in the analysis of systematic absences for the 3_1 axis in this data.

The accuracy of a model solution can also be judged by a study of the bond lengths and angles in the refined structure. Figure 7.6i–j present a summary of heavy-atom bond lengths and angles for the final anisotropic refinement in $P3_112$. Included are the mean values (with standard deviations) for each distinct bond length and angle. These bond distances are consistent with literature values[65] derived from crystallographic studies of similar organic functionalities. In addition, it is possible to compare these

values to the bond lengths and angles observed in the crystal structure of 2,9-decanedione/urea solved from room temperature data.[7] The columns at far right provide bond distances and angles obtained from this structure. It is clear that the pair of solutions are very similar. The largest discrepancy lies in the bond lengths and angles for the guest alkyl chain. For the "mixed-guest" UIC containing 2,9-decanedione and 6-chlorohexyl acetate, the carbon-carbon lengths are slightly longer (by an average of 0.040 Å, or about 3%) and the C-C-C bond angles are more acute (by an average of 4.1°, or 3.5%) than in the "pure" crystal of 2,9-decanedione/urea. These differences may be attributed to the temperatures at which the data were collected: –40 °C for the "mixed" crystal and 21 °C for 2,9-decanedione/urea. In the urea inclusion channel, the guests are relatively free to undergo several types of vibrations, translations and librations along the channel.[12] The libration of the methylene units of the guest makes carbon-carbon bonds appear shorter and "flattened" in the X-ray structure solution. (Indeed, the carbon-carbon bond distances and angles observed for both structures vary somewhat from the values expected (approximately 1.54 Å and 109.5°).) For the room temperature structure of 2,9-decanedione/urea, increased librational motion at room temperature makes the observed bond distances and angles shorter and more obtuse; at lower temperatures, this motion is suppressed so that the mixed crystal provides longer *apparent* bond lengths and smaller *apparent* bond angles.

In summary, the crystal structure determination of a UIC crystal containing a mixture of approximately 92:8 2,9-decanedione and 6-chlorohexyl acetate provides no information about the ordering of the distinct guests. The solution, either isotropic or anisotropic, consists entirely of 2,9-decanedione guest and shows no indication of excess

electron density that cannot be accounted for in a model of pure 2,9-decanedione guest. An investigation of systematic extinctions for the 3_1 screw axis provides very weak violations and provides little evidence of symmetry lowering. From this data, the reduction of the 3_1 screw by the incorporation of guest impurity is not clearly observed. This conclusion is congruent with the extremely weak birefringence exhibited by UICs grown from solutions of 2,9-decanedione and 6-chlorohexyl acetate (Figure 7.6).

7.4 Retraction of the Ultrafast Stress Strain Device

In the studies of domain reversion described in Chapter 4, the ultrafast stress-strain device was used to strain crystals in very small (usually 1 μm) increments and to remove the applied stress quickly, when necessary. This device is called "ultrafast" because of its ability to retract the applied force at a high rate of speed. Earlier studies of reversion kinetics used an analog dynamometer; for that instrument, a fast-acting solenoid was used to retract the stress bar from the crystal. However, in these studies, control over stress bar retraction was limited.[66] Potential interference from the strain device made the accurate measurement of domain reversion kinetics impossible.

The ultrafast stress-strain device was designed to overcome this problem. (The design of this instrument is outlined in Sections 4.4 and 7.6.) For the kinetics experiments described in Chapter 4, it was necessary to determine the rate of retraction of the stress bar in order to determine whether the rates of domain reversion measured by ultrafast videomicroscopy could be trusted. Because most crystals were compressed by less than 20 μm, it was only necessary to measure the rate of retraction over this distance (or slightly greater, to allow for backlash of the retracted stress bar). Because the stress

bar would oscillate about the equilibrium position following retraction, it was usually retracted by 300 μm or more so that it would not contact the crystal and interfere with domain reversion.

To measure the retraction rate, the stress bar was retracted by 400 μm and the event was captured at 10,000 frames per second. Figure 7.7 provides still images (in 0.1 ms increments) from the first few moments of the retraction. In these, the live anvil is on the left side of each image and the stationary anvil is on the right. Prior to retraction (at –0.1 ms, first frame), these stress bars are separated by approximately 80 μm. During retraction, the live stress bar moves quite quickly to the left, and motion (either in the stress device or in the microscope/recording device) makes the stationary anvil appear to move slightly to the right of the frame and oscillate over the next several frames. By measuring[67] the distance between the live anvil and stationary anvil in successive frames, the rate of retraction was calculated. The plot in Figure 7.7 provides the separation distance for the first 1.2 ms of the event. Over the first five frames (0.4 ms), the bar retracts at a constant rate of 26.8 cm s^{-1}. The bar travels at this initial rate for a distance of 107 μm. In the remaining frames the rate increases to 89.6 cm s^{-1}. For later frames the position of the bar was outside of the viewing area, so the rate of retraction is unknown.

The initial rate of 26.8 cm s^{-1} over 100 μm is fast enough so that the stress device should not influence even the fastest measured domain reversion in the crystals used, and the stress anvil should not collide with a jumping crystal. In fact, for many experiments described in Chapter 4, the stress bar is out of the viewing area (never to return) by the time appreciable domain reversion has occurred. For each of these experiments, the stress anvil was retracted by 300 μm. From the plot in Figure 7.7, the anvil should reach

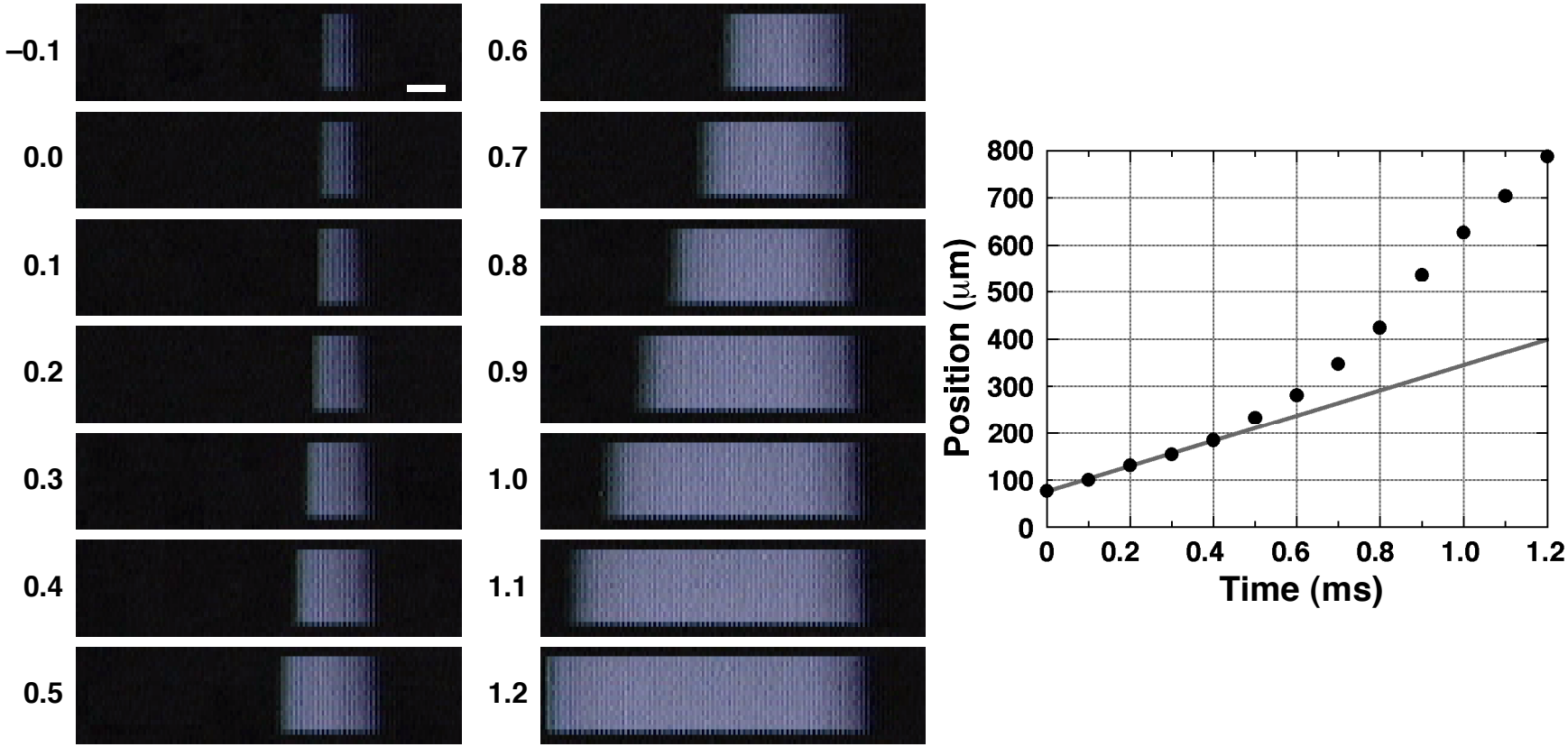

Figure 7.7 The determination of retraction rate for the ultrafast stress-strain device. Here, the unloaded stress anvil was retracted and the event recorded at 10,000 frames per second. The images at left are successive frames from this event. Time (in milliseconds from the time of retraction) is provided by the numbers to the left of each frame. Scale bar = 0.10 mm. The first evidence of anvil movement is observed in the second frame, at time = 0. For each frame, the distance between moving anvil and stationary anvil was measured and plotted vs. time in the graph at right. In the graph, the first five data points fall on a line with slope 268 μm ms^{-1}, or 26.8 cm s^{-1}. Thus, the initial rate of retraction is 26.8 cm s^{-1}. This rate is constant over the first 100 μm travelled. Over time, the rate of retraction increases: for the last five points in the graph, the average rate of retraction is 89.6 cm s^{-1}.

the end of its 300 μm retraction at approximately 0.55 ms following release; thus, anomalous changes in luminosity observed long after this period do not appear to result from retraction of the stress anvil.

7.5 Experimental Section

7.5.1 General Information:

Solvents were purified immediately before use as follows.[68] Tetrahydrofuran and diethyl ether were distilled under nitrogen from sodium-benzophenone ketyl. Dichloromethane was distilled under nitrogen from calcium hydride. Ethyl alcohol was distilled under nitrogen from magnesium ethoxide. All other solvents were of ACS reagent grade or better and were used as received unless stated otherwise. All water was distilled unless stated otherwise.

All reactions were performed in glassware that was cleaned and dried overnight in an oven. Argon and nitrogen gases were bubbled through sulfuric acid, then passed over potassium hydroxide pellets and Drierite (calcium sulfate). Drying tubes were packed with Drierite and glass wool, and dried overnight before use. Flash column chromatography was performed using 60 Å 70-230 mesh silica gel (Aldrich #28,862-4) according to the method of Still.[69] Thin-layer chromatography was performed using Analtech Silica Gel HLF plates (Analtech #47521) and visualized using one or more of several methods, including ultraviolet light (254 nm) and stains such as iodine vapor (I_2), *p*-anisaldehyde (PAA), or 2,4-dinitrophenylhydrazine (DNP). Melting points were recorded on a Thomas Hoover Melting Point Apparatus and are uncorrected. Reactions involving alkyl halides (particularly alkyl iodides) were conducted in the dark; their

workups were performed in dim light and care was taken to store the isolated products in darkened containers.

^{1}H and ^{13}C NMR spectra were recorded on a Varian Pollux 400 MHz (399.8 and 100.5 MHz, respectively) or a Varian Gemini 200 MHz (200.0 and 50.3 MHz) systems (as noted) and are referenced internally to residual protonated solvent signals: $CDCl_3$ = 7.27 and 77.27 ppm for ^{1}H and ^{13}C resonances, respectively; DMSO = 2.50 and 39.5 ppm for ^{1}H and ^{13}C resonances, respectively. NMR spectra were analyzed using Varian VNMRJ, SWAN-MR (v. 3.6.1, for Macintosh), or Spinworks (v. 2.54, for Windows).

7.5.2 Differential Scanning Calorimetry

Differential scanning calorimetry (DSC, section 3.1) was performed using a Perkin-Elmer Pyris 1 DSC. Samples were hermetically sealed in 30 μL aluminum pans. An identical empty pan was used as a reference. Most DSC runs were carried out at a heating (or cooling) rate of 10 °C min^{-1}. For experiments performed below room temperature, cooling was provided by a stream of cold N_2 from a Pyris Cryofill cooling system equipped with a liquid nitrogen dewar. The functional range of temperatures for this system is approximately –180° to +350 °C.

Instrument calibration was performed at 10 °C min^{-1} with two standard samples of high purity; these included indium and decane. The indium standard was supplied by Perkin-Elmer. Its melting point is 156.61 °C, and its enthalpy of melting is 28.45 J g^{-1} (values supplied by Pyris[70] software, v. 2.0.4.0). The decane standard (99.9% purity) was supplied by Wiley Organics (currently ChemSampCo). Its melting point is –29.7 °C.[71] The measured melting point values for these standards and the enthalpy of melting for

indium were used to calibrate the instrument's temperature and enthalpy profiles, respectively. Furnace calibration was performed typically between the temperatures of –100° and 350 °C. In cases of erratic instrument behavior, the heat-sensitive low-temperature apparatus was removed and the oven was cleaned at high temperature. An example of DSC calibration is provided on laboratory notebook page jrr-e017.

7.5.3 Guest Content Analysis

Because the precise ratio of guests in a given crystal can vary from the nominal (solution) content, individual sectors of strained crystals were cleaved with a scalpel and analyzed by high-performance liquid chromatography (HPLC) for actual guest content. Rotational twins extending over more than one growth face were cleaved, and each rotational twin was sampled individually. Segments not analyzed in the stress experiment were analyzed as well for comparison. Samples were dissolved in Acros HPLC "gradient grade" methanol.

HPLC analysis was carried out in the laboratory of Professor Christopher T. Culbertson, Chemistry Department, Kansas State University. Briefly, the system consists of a Waters 2690 autosampler and pump with Waters 486 UV detector and DuPont Zorbax ODS C18 column (4.6 mm diameter by 25 cm in length; 5 μm beads). Millenium-32 *v*. 3.05.01 software was used for device control and data analysis. A fixed eluent of 24% water, 40% acetonitrile, and 36% methanol was used. The solvents were Acros HPLC "gradient grade," and the water was deionized and filtered through a Barnsted filtration system. The instrument was set up as follows: flow rate = 1 mL/min, UV detector @ 275 nm (λ_{max} for 2,9-decanedione in the mixed solvent[72]; for 2-decanone,

λ_{max} = 276 nm), absorbance units at full scale (AUFS) = 0.05. Up to four 50 μL injections of each sample (based on sample amount, typically one injection per ~0.1 mg sample) were used; periodically a standard (containing a known ratio of guests) was injected to monitor HPLC performance and to help establish the limits of accuracy for the sample injections.

Calibration of the HPLC instrument was performed with multiple injections of samples containing different concentrations of an 80:20 mixture (in methanol) of 2,10-undecanedione and 2-undecanone or a 77:23 mixture of 2,10-undecanedione and 10-bromo-2-decanone. Calibrant injections (50 μL) were performed in a fashion identical with the crystal sample injections, and the concentrations employed were representative of the guest concentrations measured in the crystal samples (on the order of 3 mM for a 50 μL injection). The setup of this HPLC instrument is outlined on laboratory notebook page jrr-c059, and instrument calibration and sample data are found in c135.xls and c141.xls. Dilutions of the brominated guest were stored and manipulated in dark or near-dark conditions. The calibration curve for each guest was highly linear, with squared error (R^2) values of 0.999, 0.998 and 0.996 for 2,10-undecanedione (43 points), 2-undecanone (21 points) and 10-bromo-2-decanone (19 points), respectively. Figure 7.8 provides sample chromatograms and the calibration curves.

7.5.4 Microscopy

Crystals were viewed with a Nikon Microphot-SA microscope equipped with crossed polarizers and a 530 nm λ plate. Still photographs were taken with a Nikon D1 digital camera (2000 x 1312 pixel images calibrated using a reticle with 0.10 mm

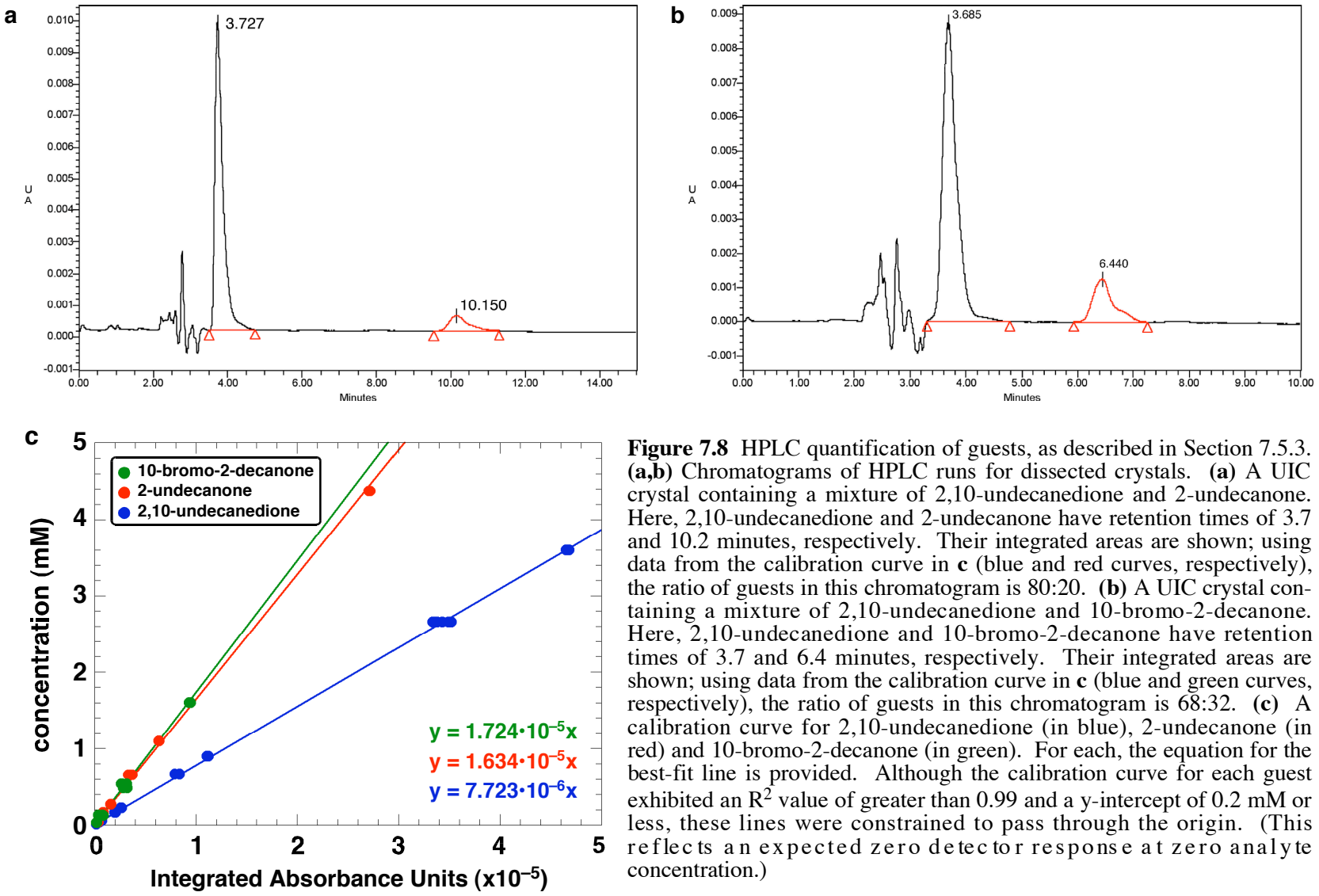

Figure 7.8 HPLC quantification of guests, as described in Section 7.5.3. **(a,b)** Chromatograms of HPLC runs for dissected crystals. **(a)** A UIC crystal containing a mixture of 2,10-undecanedione and 2-undecanone. Here, 2,10-undecanedione and 2-undecanone have retention times of 3.7 and 10.2 minutes, respectively. Their integrated areas are shown; using data from the calibration curve in **c** (blue and red curves, respectively), the ratio of guests in this chromatogram is 80:20. **(b)** A UIC crystal containing a mixture of 2,10-undecanedione and 10-bromo-2-decanone. Here, 2,10-undecanedione and 10-bromo-2-decanone have retention times of 3.7 and 6.4 minutes, respectively. Their integrated areas are shown; using data from the calibration curve in **c** (blue and green curves, respectively), the ratio of guests in this chromatogram is 68:32. **(c)** A calibration curve for 2,10-undecanedione (in blue), 2-undecanone (in red) and 10-bromo-2-decanone (in green). For each, the equation for the best-fit line is provided. Although the calibration curve for each guest exhibited an R^2 value of greater than 0.99 and a y-intercept of 0.2 mM or less, these lines were constrained to pass through the origin. (This reflects an expected zero detector response at zero analyte concentration.)

graduations) or, when specified, a Kodak DCS Pro 14n digital camera. Crystal manipulation and surgery was performed on a Meiji microscope, with still photography taken with the Nikon D1 camera. Slow (30 fps) videos were recorded using a Sony DXC-151A Hi-8 video camera and Panasonic DMR T3040 DVD recorder or a JVC BR-S925U S-VHS videocassette recorder.

Domain reversion events were captured (at frame rates of up to 10,000 fps) using either a Kodak MotionCorder SR-Ultra or an X-Stream Vision XS-4 (on loan from Speed Vision Technologies, Inc.) For video sequences collected using the MotionCorder, images were exported (via S-video) to a PC and recorded using Adobe Premiere (v. 5, for Windows). Video sequences captured using the X-Stream camera were exported to a PC and recorded using X-Stream X-Vision (v. 1.05, for Windows). Ultrafast images from both cameras were converted to QuickTime movies, and still frames were extracted using Adobe Premiere 5, X-Stream X-Vision 1.05, or Xcitex MiDAS 2.0 (all for Windows).

For images collected using the Nikon microscope, Nikon M Plan objectives were used with magnifications of 1.3×, 5×, 10×, 20× and 40×. For a microscope with good optics, the maximum achievable resolution is described by the observation wavelength (λ) and the numerical aperture (a), which describes an objective's ability to gather divergent rays of light transmitted through the specimen.[73] Using the relationship,

$$R \geq \frac{\lambda}{2a},$$

it is possible to determine the highest possible resolution (R) for a given objective, which is limited by the diffraction of light.[74] Since white light was used for the majority of studies performed in this work, an intermediate wavelength (550 nm) has been used to

estimate maximum resolving power in the table below. In practice, however, these resolutions are probably not met. For photomicrographs collected using this microscope, the image resolution (R_{exp}) was measured *per pixel* using a reticle with 0.10 mm graduations. These "per pixel" resolutions provide a scale factor by which crystal sizes could be determined.

Objective	*a*	R (at 550 nm), μm	R_{exp} (experimentally measured) μm/px	px/μm
1.3×	0.03	9	1.86	0.54
5×	0.10	2.8	0.93	1.08
10×	0.25	1.1	0.46	2.16
20×	0.40	0.69	0.23	4.28
40×	0.65	0.42	0.12	8.47

Birefringence images collected using the Metripol microscope (and Prior objectives) are subject to the same limitations in resolution. For these, the *per pixel* resolution is also limited by the 768 × 512 pixel resolution of the CCD camera used to collect the birefringence data and is less than the resolution observed in still images collected using the Nikon microscope.

Objective	*a*	R (at 550 nm), μm	R_{exp} (experimentally measured) μm/px	px/μm
1.3×	0.03	9	7.00	0.14
4×	0.10	2.8	2.08	0.48
10×	0.25	1.1	0.80	1.25
20×	0.40	0.69	0.40	2.50

The maximum resolution observed in ultrafast video images is limited by the optics of the recording devices. The *per pixel* resolutions for both cameras (measured with the 0.10 mm reticle using Nikon objectives) are provided below.

Objective	*a*	per pixel resolution, μm Kodak MotionCorder	 X-Stream XS-4
1.3×	0.03	6.0	13.9
5×	0.10	3.0	7.0
10×	0.25	1.5	3.5

7.5.5 Birefringence Mapping

Birefringence images of crystals were collected using the Metripol rotating polarizer microscope[75] built by Oxford Cryosystems. Briefly, this instrument is capable of measuring intensity, phase retardation of eigenrays (as $|\sin \delta|$) and extinction orientation of a sample at one or more of several wavelengths. When one wavelength is used, images are colored in a fashion that corresponds to the scale of first-order interference colors (as represented in a Michel-Levy chart[76]).

The instrument employed is built using a Prior polarizing microscope and optics and illumination is provided by a Nikon light source. Four different interference filters are employable, each providing a different illumination wavelength. These are 550, 580, 590 and 600 nm. For UIC crystals, the 600 nm filter was often used, although Fourier artifacts (which can accompany extremely birefringent samples) occasionally make usage of one of the other wavelengths more desirable. This technique is adequate for UICs such as those containing mixtures of 2,9-decanedione and 2-decanone, where $\arcsin|\sin \delta| = \delta$.

For UICs with large phase retardations, such as those of 2,10-undecanedione/urea (and its mixed crystals with 2-undecanone), $\arcsin|\sin \delta| \neq \delta$, and retardation images

determined from measurements at a single wavelength will not accurately reflect the retardation of the material. Overcoming this obstacle, images of absolute retardation, δ, can be obtained by combining data collected at three wavelengths.[77] This method is only applicable for sufficiently small values of δ, perhaps less than 30. For crystals based on 2,10-undecanedione/urea this precludes crystals of thickness greater than about 80 μm.

Calibration of this instrument consists of correcting for noise in the electronics by collecting a "background" image and adjusting the λ/4 plate orientation (in the absence of a sample or the analyzer) so that variation in the intensity of transmitted light is minimized. This is carried out using the supplied 10× objective, which is thought to be the freest of strain and other optical aberrations. The calibration is performed at each wavelength; errors in |sin δ| usually range from 0.02 to 0.03 for all four wavelengths. Typical calibrations are presented on laboratory notebook pages jrr-c094 and jrr-d260.

7.5.6 Stress-strain Experiments

The ultrafast stress-strain device used for kinetic studies was locally designed and built by Professor Mark Hollingsworth and members of the Electronics Design Laboratory and the Advanced Manufacturing Institute of Kansas State University. (See Figure 4.7.) In essence, it consists of a series of stacked piezoelectric transducers that can accurately control the position of a zirconia bar (the stress anvil) in 20 nm increments while measuring the applied force. Other stress-strain experiments, including those performed at Brookhaven National Laboratory, involved devices that utilized analog dynamometers. The device used in the experiment with the piezoelectric buzzer was

built in the Chemistry Department at Indiana University and followed (in part) the design of Burkhardt et al.[78]

A typical strain experiment was carried out on a Nikon Microphot-SA microscope equipped with crossed polarizers and a 530 nm λ plate. Experiments were documented by a combination of still photographs and video. Crystal size was typically 1–2 mm across by >100 μm thick (along [001]). The point of initial strain was denoted as the position where the stress reading became non-zero and no visible movement of the crystal could be identified. From photographs, the effective width of the crystal at zero strain, L_0, was measured in Adobe Photoshop (v. 5.5 for the Macintosh). The strain, S, is defined as the amount of compression of the crystal as a percentage of unstressed crystal width; it is calculated as below, where Δx is the change in stress device position (in μm) from L_0:

$$S = \frac{\Delta x}{L_0} \times 100.$$

In determining the plastic-elastic threshold, crystals were strained at room temperature to an appropriate strain in 1 μm increments. Strain release was performed in a similar fashion. Crystals whose daughters retreated fully were deemed "elastic" (at the strain achieved) and were typically strained again to a greater compression. Crystals whose daughters did not fully retreat were deemed "plastic." Following the stress-strain experiments, HPLC analyses of the crystals (described above) were performed. Figure 7.9 includes experimental parameters and source information for the stress strain experiments performed.

Figure 7.9 **(a)** Experimental parameters for the stress-strain experiments described in Section 4.4. As discussed, actual guest content (provided in the second column) was determined by HPLC of the stressed sectors. Data on crystal source (fifth column), the nominal guest content (sixth column) and information on the collection and analysis of the ultrafast video (columns seven through twelve) are provided. In the fourth column, the crystal size is designated as the width of the crystal at zero strain, L_0. In the eighth column, "K" designates use of the Kodak MotionCorder camera for ultrafast video capture, while "S" designates X-Stream XS-4. **(b)** Data for all stress experiments performed. These are described in Section 4.3.2. Here, HPLC-determined guest content, experiment page numbers and strain data are provided. The strain data are in red (for plastic behavior) or green (for pseudoelastic behavior).

a

entry	2-undecanone (% actual)	thickness (μm)	size (L_0) (μm)	crystal source	2-undecanone (% solution)	ultrafast video	Camera, objective	marquee size (μm²)	video analysis	curve fit analysis	analysis file
1	4.7	114	788	mlp-a-255-2	6	jrr-c258-25	K 5×	30 × 360	jrr-c295	jrr-f241-8	c274new.xls
2	10.8	138	559	mlp-a-232-2	14	jrr-d024-20	S 10×	56 × 280	jrr-d037	–	d037.xls
3	11.3	111	1000	mlp-a-232-2	14	jrr-d023-35	S 10×	210 × 210	jrr-d036	–	d036.xls
4	11.4	136	1060	mlp-a-236-2	12	jrr-c270-32	K 1.3×	140 × 570	jrr-c292	jrr-f242-4	c292.xls
5	11.5	160	913	mlp-a-230-2	10	jrr-c262-25	K 1.3×	72 × 560	jrr-c281	jrr-f243-3	c281new.xls
6	11.8	203	989	mlp-a-230-2	10	jrr-c267-34	K 5×	30 × 170	jrr-f081	jrr-f244-5	c288new.xls
7	12.5	157	707	mlp-a-233-3	16	jrr-d018-25	S 10×	280 × 300	jrr-f124	–	f124.xls
8	15.0	76	663	mlp-a-234-2	18	jrr-d016-33	S 10×	52 × 330	jrr-f141	–	d030.xls
9	15.0	76	663	mlp-a-234-2	18	jrr-d016-33	S 10×	70 × 420	jrr-c304	–	d031new.xls
10	15.8	221	887	mlp-a-232-2	14	jrr-d020-26	S 10×	42 × 540	jrr-d035	–	d035.xls
11	17.0	161	1620	mlp-a-235-2	20	jrr-d013-25	S 5×	210 × 1570	jrr-c302	–	d028new.xls
12	17.6	161	1620	mlp-a-235-2	20	jrr-d013-25	S 5×	98 × 1310	jrr-d026	–	d026.xls

b

2-undecanone (%)	crystal sector	stress attempt, strain (%) 1	2	3	4	5	6
4.3	jrr-c261-39	*0.62*					
4.7	jrr-c259-21	*0.76*	*0.51*	*0.24*			
7.0	jrr-d242-36	*0.63*					
7.1	jrr-d241-32	0.50	0.69				
7.5	jrr-d242-35	*0.63*					
7.6	jrr-d241-30	0.50	0.69				
7.8	jrr-d240-33	*0.54*					
7.9	jrr-d242-34	*0.63*					
8.2	jrr-d241-31	0.50	0.69				
8.3	jrr-d240-34	*0.54*					
8.9	jrr-d234-50	0.34	*0.44*				
9.1	jrr-d232-36	*0.63*					
9.9	jrr-c168-19	*0.53*					
10.0	jrr-c208b	1.91	1.91	1.80	3.70	2.70	*3.48*
10.0	jrr-c181a	1.26	1.20	1.48	0.49	*2.18*	
10.1	jrr-d219-70	0.78	1.22				
10.5	jrr-d223-76	0.78	*1.06*				
10.5	jrr-d223-77	0.78	*1.06*				
10.6	jrr-d231-52	0.66	*0.83*				
10.7	jrr-c209b	1.91	1.59	2.23			
10.7	jrr-c209c	1.91	1.59	2.23			
10.7	jrr-c184a	1.15	*2.39*				
10.7	jrr-d217-21	0.68	1.03	1.28			
10.8	jrr-d024-20	0.90					
10.9	jrr-d231-53	0.66	*0.83*				
10.9	jrr-d231-54	0.66	*0.83*				
11.0	jrr-c271b	0.85	*0.66*				
11.0	jrr-c181b	1.26	1.20	1.48	0.49	*2.18*	
11.2	jrr-c194d	1.87					
11.2	jrr-c208a	1.91	1.91	1.80	3.70	2.70	*3.48*

2-undecanone (%)	crystal sector	stress attempt, strain (%) 1	2	3	4	5
11.3	jrr-d227-45	*0.70*				
11.3	jrr-d023-35	0.90				
11.3	jrr-c184b	1.15	*2.39*			
11.4	jrr-d219-69	0.78	1.22			
11.4	jrr-c271a	0.85	*0.66*			
11.4	jrr-d229-56	0.65	0.74	*0.93*		
11.5	jrr-c264-31	0.55	0.55	0.39	0.77	0.56
11.6	jrr-d221-78	0.54	0.91	*1.03*		
11.6	jrr-c173-17	1.24				
11.6	jrr-c266a	1.21				
11.7	jrr-c191	*2.23*				
11.7	jrr-c181d	1.26	1.20	1.48	0.49	*2.18*
11.7	jrr-d217-22	0.68	1.03	1.28		
11.8	jrr-c181c	1.26	1.20	1.48	0.49	*2.18*
11.8	jrr-c267-34	1.21				
11.8	jrr-c194a	1.87				
11.8	jrr-c194a	*1.87*				
11.9	jrr-d219-71	0.78	1.22			
12.0	jrr-c209a	1.91	1.59	2.23		
12.1	jrr-d219-72	0.78	1.22			
12.1	jrr-d223-75	0.78	*1.06*			
12.2	jrr-d217-20	0.68	1.03	1.28		
12.3	jrr-d221-79	0.54	0.91			
12.3	jrr-c194b	1.87				
12.3	jrr-d221-77	0.54	0.91	*1.03*		
12.3	jrr-c194b+c	*1.87*				
12.5	jrr-d018-25	*2.12*				
12.5	jrr-d229-57	*0.93*				
12.7	jrr-c198-2a	1.97	*3.0*			
12.7	jrr-c198-3b	1.97	3.0			

2-undecanone (%)	crystal sector	stress attempt, strain (%) 1	2	3	4	5
12.8	jrr-d229-58	0.93				
12.8	jrr-d237-5a	0.65	0.74	*0.93*		
13.1	jrr-d252-20	*2.58*				
13.4	jrr-d251-19	*2.76*				
13.9	jrr-d251-18	2.76				
14.1	jrr-d256-40	2.25	1.93	*2.71*		
14.1	jrr-d250-31	3.25				
14.2	jrr-d254-27	*3.01*				
14.3	jrr-d148-96	0.50	1.05	1.50		
14.3	jrr-c170-7	2.70				
14.3	jrr-d251-17	2.76				
14.3	jrr-d252-21	2.58				
14.4	jrr-d254-28	*3.01*				
14.8	jrr-d149-40	1.20	1.92			
15.0	jrr-d256-41	2.25	1.93	*2.71*		
15.0	jrr-d016-33	1.96				
15.2	jrr-d257-13	*2.52*				
15.3	jrr-d264-13	1.80	2.41	2.77		
15.5	jrr-d264-14	1.80	2.41	2.77		
15.5	jrr-d148-98	0.50	1.05	1.50		
15.8	jrr-d020-26	0.68				
15.9	jrr-d266-68	2.81				
16.1	jrr-d266-67	2.81				
17.0	jrr-d013-25	1.05				
17.4	jrr-d268-69	2.57				
17.6	jrr-d013-25	1.05				
18.9	jrr-d268-70	2.57				
19.3	jrr-d268-68	2.57				
21.2	jrr-d157-39	2.49				
22.1	jrr-d159-55	2.48				

The acoustomechanical relaxation experiments were performed by the placement of a Radio Shack 12VDC Piezo Mini Buzzer (Part number 273-074, 4.1 kHz primary frequency, with other frequencies of significant intensity) on the microscope stage or on the goniometer mounted stress-strain device (Section 5.2). In each case the buzzer was oriented so that the primary direction of sound output was along the channel axis of the crystal [001]. The sound pressure output for this device is rated at 70 dB min at 30 cm and 12 VDC. (Several different buzzers were used, and one of these emitted a noticeably weaker output. This device was not used in the *in situ* stress-diffraction experiments described in Chapter 5.)

In situ stress diffraction experiments (described in Chapter 5) were conducted using a goniometer-mountable stress strain device that was designed and built by Professor Mark Hollingsworth and members of the Electronics Design Laboratory and the Advanced Manufacturing Institute of Kansas State University. (See Figure 4.7.) In this experiment, the crystal is glued to one of the nylon stress bars, and stress is applied using an actuator controlled by a thumbscrew. While under stress, X-ray rotation images were collected on a Bruker SMART1000/P4 single crystal diffractometer. Details specific to each experiment, including X-ray data collection parameters, are described in Chapter 5.

In experiments conducted to measure the kinetics of domain reversion, the crystal was oriented so that the mother domain was in the extinguishing position, and the daughter was approximately 60° from this. This arrangement was preferred to the alternative, in which the daughter was in the extinguishing position. For a crystal oriented as such, retreat of the daughter domain results in an increase in luminosity. The

orientation of the mother domain in the extinguishing position allowed facile identification of the orientation states populated in any given stress experiment. However, as illustrated in Figures 3 and 4 in Brown and Hollingsworth,[79] the occurrence of a third domain orientation, which is oriented 60° from both daughter and mother (see Chapter 5), is an additional possibility. For a crystal oriented so that the mother is in the extinguishing position, reversion from either daughter or the third orientation (both to the mother) will give rise to a decrease in luminosity so that these processes are indistinguishable in the kinetic data. By rotating the stressed crystal 60° away from the extinguishing position for daughter or mother, one may observe the third orientation and take steps to avoid confusing reversion from this and the daughter domains. Although this was not performed for the kinetics experiments described (movement of the microscope stage, which could disturb the stressed crystal, was avoided), only a small fraction of the daughters formed contain significant amounts of the third orientation. Nevertheless, the rates provided in Section 4.4 should be considered upper limits for the rate of daughter to mother reversion. (However, they should still be considered domain reversion rates.) In addition, this treatment assumes the daughter spans the entire thickness of the crystal. Fortunately, rotational twinning along the channel axis is thought to disfavorable on the grounds that such twins could not preserve epitaxy with their surroundings, and this effect is not expected to contribute to the measured rates.

Domain reversion kinetics were determined by observing changes in crystal luminosity. As discussed in Section 4.4, the volume V_0 of daughter observed *before* stress release (time = 0) was calculated using the following expression:

$$V_0 = \frac{a \times \ell \times \bar{x}_0}{R^2}. \qquad (1)$$

In the numerator, a denotes the marquee sample area (expressed in px^2; see Section 4.4 and Figure 7.9), ℓ denotes the crystal thickness (in μm) and $\bar{x}_0$ is the fraction of the sample area occupied by daughter (discussed below). In the denominator, R is the resolution of the recorded image (measured using a reticle and expressed in pixels μm^{-1}; see Section 7.6.4).

For each experiment it is important to determine the fraction of sample area populated by daughter domain ($\bar{x}_0$) prior to domain reversion. In each case, the high contrast between extinguished mother regions and transmitting daughter regions allowed this to be achieved using the magic wand tool in Adobe Photoshop. This function allows the selection of pixels exhibiting similar luminosities within a threshold that is set by the user (using a scale of 1 to 255). Differences in image quality and saturation recorded for each experiment demanded that the threshold value be varied between determinations, although it was typically set at 40 or less. (Only very similar pixels were selected.) In each case, the regions selected by the wand tool were visually inspected, and adjustments were made so that the mother and daughter domains were accurately defined.

At any time in the reversion experiment, the volume of daughter (calculated using Equation 1) can be used to calculate the number of moles of guest in the daughter domain:

$$\text{moles} = \frac{4V}{V_{2,10} \times n}. \qquad (2)$$

Here, $V_{2,10}$ is the volume of one unit cell and n is Avogadro's number. (Here, the cell constants[79] for 2,10-undecanedione/urea were used; see Figure 1.3), The multiplier 4 provides units of moles of guest (there are 4 guests per unit cell). By determining the moles of daughter present before ($moles_0$) and following ($moles_f$) domain reversion, one identifies the contribution of daughter domain to the observed luminosity:

$$Z = \frac{(moles_0 - moles_f)}{(L_0 - L_f)} = \frac{\Delta moles}{\Delta L}. \qquad (3)$$

Here, L_0 and L_f are initial and final luminosities, respectively. (This assumes a linear correspondence between these two quantities; see Section 4.4 and references therein.[80,81])

Since Z expresses the relationship between the observed luminosity and the amount of daughter domain, it is a simple matter to determine the number of moles of daughter at any time (t):

$$moles_t = Z \times L_t. \qquad (4)$$

By dividing the *change* in moles of guest between successive frames by the time elapsed between those frames,

$$rate_t = \frac{\Delta moles_t}{\Delta t}. \qquad (5)$$

one obtains an instantaneous rate of reversion in moles of guest s^{-1}.

For example, domain reversion for entry 1 (4.7% 2-undecanone) was captured using the Kodak MotionCorder and a 5× objective (3.00 μm/pixel resolution; Section 7.6.4). Using a sample marquee with a = 1190 px^2, daughter fraction $\bar{x}_0$ = 0.437 and crystal thickness $\ell = 113_8$ μm, daughter volume $V_0 = 5.33 \times 10^5$ μm^3 (Equation 1). At this time, the daughter domain contains 9.20×10^{-10} moles guest (Equation 2). Over the

course of the domain reversion experiment, luminosity decreases by 52.46 units, so (L_0 – L_f) = 52.46 and Z = 1.75 × 10^{-11} moles of guest per luminosity unit (Equation 3). This value, which scales luminosity to daughter population, can then be used to determine the number of moles (guest) in every recorded frame in this experiment.

To determine the rate of reversion between, for instance, time = 38 and 39 ms, one must first identify the moles of daughter observed in those frames. For these, the normalized luminosities, ΔL_t, are 55.20 and 55.02 units, respectively. Using Equation 3, the number of moles of guest observed in the daughter domain at t = 38 ms is 9.67 × 10^{-10}; at t = 39 ms, this quantity decreases to 9.64 × 10^{-10}. Over the 1 ms time span between these frames, 3.17 × 10^{-12} moles of guest revert at an observed rate of 3.17 × 10^{-9} moles of guest s^{-1} (Equation 5). Similar calculations were carried out using data from each video image using Microsoft Excel. The file names are provided in Figure 7.9.

7.6 Synthetic Procedures

2,7-octanedione (jrr-a077): 2,7-Octanedione was prepared according to the method of Brown, *et al.*[2] In a 250 mL Erlenmeyer flask, red HgO (1.08 g, 5.00 mmol, Baker, 99.7%) was stirred with water (20 mL). To this, concentrated sulfuric acid (10 mL, 18 mmol) was dripped into the mixture, with rapid stirring and the evolution of heat. The red HgO powder almost completely dissolved, and the solution became colorless. This solution was decanted with stirring into a 500 mL 3-necked flask that contained a solution of 2,7-octadiyne (3.70 g, 34.9 mmol, Wiley, 98%), CH_3OH (100 mL) and water (50 mL) and had been fitted with a thermometer, a condenser and a ground glass stopper. On completion of this addition, the solution was creamy yellow in color, and the

temperature was 35 °C. The solution was heated to 60 °C over 10 minutes, at which point it became colorless. At this time, TLC indicated product formation.

The reaction was allowed to proceed for 25 minutes, after which the solution was poured into brine (200 mL) and allowed to stir for 30 minutes. The cloudy mixture was extracted with Et_2O (4 × 75 mL) and the extracts were combined to yield a clear, colorless solution with some solids present (perhaps HgO). The organic extract was washed with brine and dried over Na_2SO_4, then concentrated on a rotary evaporator to yield 5.25 g of a yellow oil with some white solids (perhaps Na_2SO_4). Short-path distillation at 3 torr and 95 °C (vapor temperature) yielded liquid and blue crystals. NMR (jrr-a079-7) of this material indicated product and impurity. The mixture was dissolved in CH_3OH and concentrated on a rotary evaporator; upon standing five days, a yellow liquid and crystals were noted. The sample was distilled at 2.2 torr and 86 °C to yield 2.720 g white crystals (with slight impurity by TLC) and 0.220 g white crystals (pure by TLC). mp 42–43 °C (jrr-e262-1). (Brown, et al. reported[2] 39.5–40.0 °C.) TLC (4:1 hexanes:EtOAc) $R_f = 0.18$ (I_2, PAA) and 0.22 (impurity in larger fraction only); ^{1}H NMR of larger fraction (400 MHz, $CDCl_3$, jrr-a079-10) 2.45 (m, 4H, COC**H**$_2$CH_2, virtual coupling), 2.14 (s, 6H, C**H**$_3$CO), 1.56 (m, 4H, COCH_2C**H**$_2$, virtual coupling); ^{13}C NMR of impure (blue) sample (50.3 MHz, $CDCl_3$, jrr-a079-8) δ 208.59, 96.96, 43.37, 29.87, 23.18.

1-methylcyclohexanol (jrr-b017): 1-Methylcyclohexanol was prepared according to a method adapted from Williamson.[82] Cyclohexanone (4.299 g, 43.79 mmol, distilled at jrr-b016) and freshly distilled Et_2O (approximately 100 mL) were placed in an argon-

flushed 200 mL round-bottom flask. With stirring, a solution of methylmagnesium bromide (29.2 mL, 87.6 mmol, 3.0 M in Et_2O, Aldrich, 99.9%) in Et_2O (20 mL) was added dropwise. The ensuing reaction caused heating and some reflux, so the flask was chilled in ice. This slightly cloudy, yellow, solution was allowed to stir 30 minutes, an argon-flushed reflux condenser was added, and the solution was refluxed for four hours. At this time, TLC indicated the presence of cyclohexanone reactant, so the solution was refluxed for an additional 90 minutes. After 5.5 hours total reflux time, the solution was poured into ice cold HCl (180 mL, 1 M) and allowed to stir overnight in an ice water bath.

After 15 hours, two clear, colorless layers were noted in the reaction flask. The upper organic fraction was collected using a separatory funnel and was set aside. The aqueous fraction was washed with Et_2O (3 × 125 mL), and all organic fractions were combined. The combined fractions were washed twice with water and once with brine to yield a clear, colorless solution. TLC of this layer indicated several impurities. The mixture was dried over $MgSO_4$, filtered, and concentrated on a rotary evaporator to yield 5.07 g of a light yellow oil. (NMR of this fraction suggested a fairly clean product; see jrr-b018-4.) Short path distillation was performed at 10 torr. The initial fraction (340 mg collected at 55–56 °C) was discarded. A second fraction, collected at 55–58 °C, consisted of 2.040 g (40.8%) of a clear, colorless liquid. TLC (4:1 hexanes:EtOAc) R_f= 0.42 and 0.49 (PAA); ^{1}H NMR (400 MHz, $CDCl_3$, jrr-b019-9) 1.7–1.2 (m, 10H, $(CH_2)_5$), 1.19 (s, 3H, CH_3).

7-bromo-2-heptanone (jrr-b025): 7-Bromo-2-heptanone was prepared according to a modified procedure of Zhang, *et al.*[83] In a dry, argon-flushed, round-bottom flask, 1-methylcyclohexanol (343 mg, 3.00 mmol, jrr-b019-7) was diluted with freshly distilled CH_2Cl_2 (20 mL). After cooling the solution in an ice bath, K_2CO_3 (3.18 g, 23.0 mmol) was added, and the mixture was allowed to stir for 10 minutes. At this point, Br_2 (2.4 g, 15 mmol, Acros, 99.8%) was added dropwise via Pasteur pipette. The mixture was allowed to stir in the ice bath for 8 hours.

A saturated solution of $Na_2S_2O_3$ (50 mL) was added to the reaction flask. The reaction mixture, still chilled, was allowed to stir for a few additional minutes. Upon standing, the milky yellow mixture separated into organic and aqueous fractions. These were separated in a separatory funnel, and the organic fraction was washed with another portion of saturated $Na_2S_2O_3$ (50 mL). This mixture was allowed to stand overnight, during which it separated into two fractions. The fractions were separated, and the aqueous portion was extracted with CH_2Cl_2 (2 × 50 mL). The combined organic fractions (clear and colorless, with some yellow solids) were washed with Barnsted-filtered water and brine before drying over $MgSO_4$. Decolorizing carbon (2 mL) was added to the $MgSO_4$ suspension, and the mixture was allowed to stand for 30 minutes. This was filtered and concentrated on a rotary evaporator to yield a light yellow oil and yellow solids. (Attempts to dissolve the solids in Et_2O or hot EtOH were unsuccessful.) The solids were removed by dissolving the oil in cold EtOH, filtration on a Büchner funnel, and then passage through a small plug of silica gel. The EtOH was removed on a rotary evaporator (with heating to 50 ºC, which appears to have induced a color change from colorless to yellow) to yield 540 mg (93.2%) of a light yellow oil. TLC (4:1

hexanes:EtOAc) R_f = 0.49 (I_2, DNP); ^{1}H NMR (400 MHz, $CDCl_3$, jrr-b031-8) δ 3.413 (t, 2H, J = 6.6 Hz, Br$C\mathbf{H}_2CH_2$); 2.461 (t, 2H, J = 7.2 Hz, $C\mathbf{H}_2COCH_3$); 2.149 (s, 3H, $COC\mathbf{H}_3$); 1.874 (2H, q, 2H, J = 7.2 Hz, $BrCH_2C\mathbf{H}_2$); 1.608 (q, 2H, J = 7.5 Hz, $C\mathbf{H}_2CH_2CO$); 1.444 (2H, m, 6.9 Hz, $BrCH_2CH_2C\mathbf{H}_2$).

2,9-decanedione (jrr-e134): 2,9-Decanedione was prepared according to the procedure of Hollingsworth, *et al.*[7] A 1 L, 3-necked flask was fitted with a thermometer, condenser and a 500 mL addition funnel. Red HgO (2.60 g, 12.0 mmol, Baker, 99.7%) and water (100 mL) were added to the flask. With rapid stirring, concentrated sulfuric acid (45 mL, 810 mmol, 18 M) was added. Evolution of heat (to approximately 75 °C) accompanied the dissolution of the HgO, and the solution turned colorless. This solution was allowed to cool to approximately 60 °C, and a solution of 2,9-decadiyne (27.97 g, 184.5 mmol, mixture of Chemsampco, 97% and K & K, unknown purity) and CH_3OH (350 mL) were added over a period of 2 hours. The solution was stirred 5.5 hours at 55–66 °C, at which time it was cloudy and yellow in appearance.

The reaction mixture was transferred to a 1L, single neck flask using Et_2O (100 mL), concentrated on a rotary evaporator until most of the organic fraction was thought to be removed, and then poured into a separatory funnel. The mixture was extracted with Et_2O (4 × 100 mL), and the organic extracts (some foamy) were combined to yield a yellow solution that was washed with water (200 mL) and brine (200 mL). The organic fraction was boiled (for 30 seconds) with three large spatula portions of decolorizing carbon and allowed to stand. Upon settling, the light yellow solution was filtered on a Büchner funnel through diatomaceous earth (Celite 521, Sigma) to produce a yellow

solution that was concentrated on a rotary evaporator. The resulting yellow oil produced crystals upon agitation. Recrystallization from boiling *n*-pentane (200 mL) produced crystals that were inseparable from a yellow oil. The entire mixture was dissolved in hexanes (500 mL) and boiled for 5 minutes with 12 g decolorizing carbon and allowed to settle, then filtered (while at approximately 30°). The nearly colorless solution was concentrated on a rotary evaporator to yield 18.10 g (51.0%) white crystals. mp 56–57 °C (jrr-e262-2) (Peppe, et al. reported[84] 52-53 °C for material synthesized via alkyne hydration). TLC (4:1 hexanes:EtOAc) R_f = 0.15 (I_2, UV); ^{1}H NMR (400 MHz, $CDCl_3$, jrr-e135-8) δ 2.417 (t, 4H, J = 7.6 Hz, COC**H$_2$**CH$_2$), 2.130 (s, 6H, C**H$_3$**CO), 1.578 (m, 4H, COCH$_2$C**H$_2$**), 1.289 (m, 4H, COCH$_2$CH$_2$C**H$_2$**); ^{13}C NMR (100 MHz, $CDCl_3$, jrr-e135-8) δ 209.3, 43.9, 30.1, 29.2, 23.9.

6-bromohexyl acetate (jrr-a011). 6-Bromohexyl acetate was prepared according to a modified procedure of Brown.[85] A nitrogen-flushed 10 mL round-bottom flask containing 6-bromo-1-hexanol (0.65 mL, 5.0 mmol, Aldrich, 97%) was chilled in an ice bath and acetic anhydride (0.73 mL, 7.7 mmol, Fisher, ACS reagent) was added all at once with stirring. The flask was attached to a nitrogen-flushed reflux condenser and warmed (with stirring) in an oil bath at 65–70 °C for 25 hours. At this time, the clear yellow solution was allowed to stand at room temperature for 4 days.

The reaction mixture was diluted to approximately 25 mL with Et_2O, washed with 1 M $NaHCO_3$ (3 × 25 mL) and then dried with brine before drying over $MgSO_4$ to yield a clear, colorless solution. Concentration on a rotary evaporator yielded 955 mg (86.1%) of clear, colorless, oil. TLC (4:1 hexanes:EtOAc) R_f = 0.46 (I_2); ^{1}H NMR (400 MHz,

$CDCl_3$, jrr-a012-4) δ 4.060 (t, 2H, J = 6.8 Hz, $BrC\mathbf{H}_2CH_2$); 3.417 (t, 2H, J = 6.8 Hz, $C\mathbf{H}_2OCOCH_3$); 2.055 (s, 3H, $OCOC\mathbf{H}_3$); 1.875 (q, 2H, J = 7.0 Hz, $BrCH_2C\mathbf{H}_2$); 1.649 (q, 2H, J = 7.0 Hz, $C\mathbf{H}_2CH_2OCOCH_3$); 1.490 (q, 2H, J = 7.8 Hz, $BrCH_2CH_2C\mathbf{H}_2$); 1.402 (q, 2H, J = 6.8 Hz, $BrCH_2CH_2CH_2C\mathbf{H}_2$); ^{13}C NMR (50.3 MHz, $CDCl_3$, jrr-a012-4) δ 171.5, 64.6, 34.0, 32.9, 28.7, 28.0, 25.4, 21.3.

6-chlorohexylacetate (jrr-a016). 6-Chlorohexyl acetate was prepared according to a modified procedure of Brown.[85] A nitrogen-flushed 5 mL round-bottom flask containing 6-chloro-1-hexanol (0.75 mL, 5.6 mmol, Aldrich, 96%) was chilled in an ice bath and acetic anhydride (0.74 mL, 7.9 mmol, Fisher, ACS reagent) was added dropwise with stirring. The flask was attached to a nitrogen-flushed reflux condenser and warmed (with stirring) in an oil bath at 65–70 °C for 22 hours.

At this time, the colorless, slightly cloudy reaction mixture was diluted to 25 mL with Et_2O, washed with 1 M $NaHCO_3$ (3 × 25 mL) and dried with brine before drying over $MgSO_4$. Concentration on a rotary evaporator yielded 992 mg of a clear, colorless, oil. NMR analysis (jrr-a016-2) indicated a small amount of impurity that was thought to be acetic anhydride (^{1}H δ = 2.225 ppm). The impure oil was again diluted to 25 mL with a 1:1 mixture of Et_2O and hexanes, washed with 1 M $NaHCO_3$ (3 × 25 mL) and brine (25 mL) before drying over Na_2SO_4. The solution was concentrated on a rotary evaporator and allowed to stand, yielding 854 mg (85.1%) of a clear, colorless oil. TLC (4:1 hexanes:EtOAc) R_f = 0.42 (I_2, PAA); ^{1}H NMR (200 MHz, $CDCl_3$ jrr-a020-3) δ 4.064 (t, 2H, J = 6.6 Hz, $CO_2C\mathbf{H}_2CH_2$), 3.541 (t, 2H, J = 6.6 Hz, $CH_2C\mathbf{H}_2Cl$), 2.050, (s, 3H,

C**H$_3$**CO$_2$), 1.9–1.3 (m, 8H, CO$_2$CH$_2$(C**H$_2$**)$_4$CH$_2$Cl); ^{13}C NMR (50.3 MHz, CDCl$_3$ jrr-a020-3) δ 171.5, 64.6, 45.2, 32.7, 28.7, 26.8, 25.5, 21.3.

5-iodopentylacetate (jrr-b037). In a dried, argon-flushed, 100 mL round-bottom flask, 5-chloropentylacetate (3.17 g, 19.5 mmol, Lancaster, 98%) was added to NaI (5.85 g, 39 mmol, Fisher, oven-dried), and the mixture was diluted with acetone (25 mL, dried over 4 Å sieves). A reflux condenser with drying tube was attached, and the solution was allowed to reflux in the dark for 120 hours, during which a majority of the solvent was lost and the solution turned brown, with yellow solids.

At this time, the reaction contents were transferred to a separatory funnel using EtOAc and water. The organic layer was separated from the aqueous fraction and then washed with water (3 × 100 mL); it remained brown. The organic fraction was swirled with approximately 5 mL decolorizing carbon, filtered, and concentrated on a rotary evaporator to yield a yellow oil. The oil was eluted through a 4 cm (o.d.) by 3 cm (long) silica plug using EtOAc solvent. The eluate was concentrated on a rotary evaporator and then to 4 torr to yield 4.30 g of a yellow oil. (^{1}H NMR of this sample demonstrated contamination with trace EtOAc.) TLC (4:1 hexanes:EtOAc) R_f = 0.60 (UV, I_2, DNP); ^{1}H NMR (400 MHz, CDCl$_3$, jrr-b037-5) δ 4.069 (t, 2H, J = 7.2 Hz, CO$_2$C**H$_2$**CH$_2$), 3.196 (t, 2H, J = 7.6 Hz, CH$_2$C**H$_2$**I), 2.055 (s, 3H, C**H$_3$**CO$_2$CH$_2$), 1.857 (q, 2H, J = 7.6 Hz, C**H$_2$**CH$_2$I), 1.638 (m, 2H, CO$_2$CH$_2$C**H$_2$**CH$_2$), 1.476 (q, 2H, J = 7.2 Hz, CO$_2$CH$_2$CH$_2$C**H$_2$**CH$_2$); ^{13}C NMR (50.3 MHz, CDCl$_3$, jrr-b037-5) δ 171.3, 64.3, 33.2, 27.7, 27.1, 21.2, 6.7.

1,7-dichloroheptane (jrr-b070). 1,7-dichloroheptane (230 g, Chemsampco, 72%) was purified by distillation at ambient pressure from an argon-flushed, 500 mL round-bottom flask fitted with a 15 cm Vigreux column and side arm distillation head. The process was conducted in dim light. The first fraction (approximately 75 mL), collected at vapor temperature = 172 °C, was discarded; a second fraction (approximately 140 mL) was collected at vapor temperature = 216 °C. The second fraction was redistilled at vapor temperature = 216 °C, and the first 15 mL portion was discarded. A second 115 mL portion was collected at vapor temperature = 216 °C and stored in an argon-flushed, darkened glass bottle. This fraction was a clear, colorless, liquid. TLC (4:1 hexanes:EtOAc, jrr-b077-4) R_f = 0.63 (UV, I_2); ^{1}H NMR (200 MHz, $CDCl_3$, jrr-b070-7) δ 3.546 (t, 4H, J = 6.8 Hz, $ClC\mathbf{H_2}CH_2$), 1.788 (m, 4H, $ClCH_2C\mathbf{H_2}CH_2$), 1.464 (q, 4H, J = 7.4 Hz, $ClCH_2CH_2C\mathbf{H_2}$); 1.354 (m, 2H, $ClCH_2CH_2CH_2C\mathbf{H_2}$); ^{13}C NMR (100 MHz, $CDCl_3$, jrr-b070-7) δ 45.2, 32.8, 28.6, 27.0.

1,7-diiodoheptane (jrr-b077). In a dried, argon-flushed 100 mL round-bottom flask, 1,7-dichloroheptane (5.121 g, 30.29 mmol, jrr-b070-6) was mixed with NaI (18.2 g, 126 mmol, Fisher, oven-dried) and acetone (50 mL, dried over 4 Å sieves). The flask was fitted with an argon-flushed reflux condenser and drying tube (filled with Drierite), and the mixture was refluxed in the dark for 24 hours.

At this time, the creamy yellow solution was allowed to cool for 4 hours. Upon chilling with ice water, an orange precipitate was observed. The solution was allowed to warm to room temperature before it was filtered on a Büchner funnel and washed with acetone (100 mL, dried over 4 Å sieves). The filtrate was orange, and white solids were

observed on the filter paper. The filtrate was concentrated on a rotary evaporator (some acetone remained) and was transferred with Et_2O and water to a separatory funnel. The material was washed with water (3 × 100 mL) and dried over $MgSO_4$ to yield a clear organic fraction. This fraction was concentrated on a rotary evaporator and allowed to stand, uncovered, for two days to yield 9.970 g (93.5%) of a light orange liquid. NMR analysis (jrr-b077-4) confirmed the presence of ~2% of peaks alpha to a chlorine, suggesting that the final product contained approximately 4% of 1,-chloro-7-iodoheptane. TLC (4:1 hexanes:EtOAc) R_f = 0.63 (UV, I_2); ^{1}H NMR (400 MHz, $CDCl_3$, jrr-b077-4) δ 3.198 (t, 4H, J = 6.8 Hz, IC**H$_2$**CH_2), 1.833 (t, 4H, J = 6.8 Hz, ICH_2C**H$_2$**CH_2), 1.5-1.3 (m 6H, ICH_2CH_2C**H$_2$C H$_2$C H$_2$**); ^{13}C NMR (50.3 MHz, $CDCl_3$, jrr-b077-4) δ 33.6, 30.5, 27.7, 7.3.

2,10-undecanedione (jrr-a099, jrr-b033). 2,10-Undecanedione was prepared according to the method of Geiger.[86] Sodium ethoxide (14.95 g, 219.0 mmol, Acros, 96%) and freshly distilled EtOH (200 mL) were added to a 1 L, 3-necked round-bottom flask that was fitted with a thermometer, condenser and an addition funnel. With stirring, the NaOEt dissolved in ten minutes to yield a clear, brown, solution. (At this time, the temperature of the solution was noted as approximately 45 °C.) Ethylacetoacetate (37.0 mL, 290 mmol, Acros, 99%) was dripped into this solution over 10 minutes (with rapid stirring, T ~ 30 °C) before heating the solution to reflux (82 °C). Once at reflux, a solution of 1,5-dibromopentane (16.84g, 73.24 mmol, Acros, 97%) in distilled EtOH (15 mL) was added over 20 minutes using an addition funnel. (Dilution with EtOH was performed after some of the dibromopentane had first been added as a neat liquid.) The

stirred reaction was allowed to reflux under argon for 4 hours, at which time NMR analysis of an aliquot (jrr-a099-6) indicated the disappearance of dibromopentane reagent. At five hours reaction time, the solution was allowed to cool to room temperature; this yielded a white precipitate and a yellow liquid.

After cooling for one hour, the solution was transferred to a 3 L round-bottom flask and diluted with Barnsted-filtered water (2 L); 1 M NaOH (600 mL) was added quickly and the solution was allowed to stir 1.5 days at 28–35 °C. After this time the cloudy orange solution was chilled to approximately 5 °C in an ice bath; concentrated HCl (90 mL, ~12.1 M, Fisher) was added over approximately 1 hour. The solution was allowed to warm as the ice melted (overnight). After 54 hours, the solution was cloudy yellow in appearance, with yellow and white solids noted on the interior of the flask. Using a large separatory funnel, the mixture was extracted with Et_2O (5 × 300 mL). The combined organic extracts were washed with water (500 mL) and brine (750 mL) before drying over $MgSO_4$ to yield a clear, colorless solution. The solution was concentrated on a rotary evaporator to yield 16.30 g of yellow solids. TLC analysis (9:1 EtOAc:MeOH, jrr-a106-13) of the material showed product (R_f = 0.62) and an impurity (R_f = 0.32). Following unsuccessful attempts at purification using decolorizing carbon, or by crystallization from hexanes, the sample was purified in three fractions. Fraction 1 (jrr-a263-5) was eluted (in approximately 15 mL THF) through a plug of silica gel; concentration on a rotary evaporator yielded 700 mg of white solids. Fractions 2 and 3 were passed through the same silica gel plug but retained their yellow color. Fraction 2 (~5.3 g, jrr-b033-1) was crystallized from boiling hexanes (50 mL). Cooling, filtration and concentration on a rotary evaporator yielded 4.95 g white powder. Fraction 3 (~1 g,

jrr-b033-3) was crystallized from boiling hexanes (10 mL). Cooling, filtration and concentration on a rotary evaporator yielded 755 mg white powder. Total yield = 6.41 g (47.5%). TLC (4:1 hexanes:EtOAc, Fraction 2, jrr-b033-2) R_f = 0.35 (I_2, DNP); ^{1}H NMR (400 MHz, $CDCl_3$, jrr-b033-2) δ 2.419 (t, 4H, J = 7.4 Hz, COC**H$_2$**CH$_2$), 2.138 (s, 6H, C**H$_3$**CO), 1.564 (q, 4H, J = 6.6 Hz, COCH$_2$C**H$_2$**), 1.288 (m, 6H, COCH$_2$CH$_2$C**H$_2$**C**H$_2$**C**H$_2$**; ^{13}C NMR (50.3 MHz, $CDCl_3$, of impure Fraction 2, jrr-a264-7) δ 209.5, 43.9, 30.1, 29.4, 29.2, 23.9.

10-hydroxy-2-decanone (jrr-b106). 10-Hydroxy-2-decanone was prepared according to a method adapted from Geiger.[86] A solution of NaOEt (3.01 g, 44.3 mmol, Acros, 96%) and freshly distilled EtOH (~20 mL) was stirred in an argon-flushed, 3-necked round-bottom flask that had been fitted with a thermometer, reflux condenser and addition funnel. A solution of ethyl acetoacetate (8.42 mL, 66.4 mmol, Acros, 99%) in distilled EtOH (~40 mL) was added in one portion, and the reaction was heated to boiling. Once all of the NaOEt had dissolved, a solution of 7-bromo-1-heptanol (4.32 g, 22.1 mmol, Aldrich, 95%) in EtOH (50 mL, distilled) was added over 5 minutes and the reaction mixture was refluxed overnight.

After 18 hours at reflux, NMR analysis of an aliquot (jrr-b106-3) indicated disappearance of the bromoalcohol starting material. At this point, NaOH (80 mL, 2.5 M) was added, and the cloudy orange solution cleared up instantly. The reaction mixture was refluxed for an additional 15 h to yield a dark brown solution with light solids. At this time, the solution was allowed to cool to room temperature and was then chilled in ice water. Upon dropwise addition of HCl (40 mL, 6 M), the solution bubbled and

became dark brown. Following this addition, the reaction mixture was allowed to warm to room temperature to yield a cloudy brown solution with a small amount of solids.

Approximately 100 mL of the reaction mixture was removed via rotary evaporation. The solution was washed with EtOAc (3 × 150 mL) and the combined organic extracts were washed with Barnsted-filtered water (2 × 150 mL) and brine (150 mL) to yield a clear, brown solution. Drying over $MgSO_4$ and concentration on a rotary evaporator yielded 4.54 g of brown oil. The oil was transferred to a 10 mL round-bottom flask and purified via short path distillation. A light yellow liquid was collected at 129.5 °C and 0.75 torr. This material, which contained some impurities by NMR, melts near room temperature. Yield = 2.47 g (64.8%). TLC (4:1 hexanes:EtOAc) R_f = 0.23 (DNP, PAA); ^{1}H NMR (200 MHz, $CDCl_3$, jrr-b110-10) δ 3.647 (t, 2H, J = 6.4 Hz, $CH_2C\mathbf{H_2}OH$), 2.425 (t, 2H, J = 7.6 Hz, $COC\mathbf{H_2}CH_2$), 2.142 (s, 3H, CH_3CO), 1.7-1.5 (m, 6H), 1.4-1.2 (m, 6H); ^{13}C NMR (50.3 MHz, $CDCl_3$, jrr-b105-11 – a different sample made using a similar synthetic method) δ 209.6, 63.3, 44.0, 33.0, 30.1, 29.6, 29.5, 29.3, 25.9, 24.0.

10-bromo-2-decanone (jrr-c014). In dim light, triphenylphosphine (1.67 g, 6.38 mmol, Aldrich, 99%) was dissolved into freshly distilled CH_2Cl_2 (15 mL) in an argon-flushed round-bottom flask. The flask was chilled in ice water, and 10-hydroxy-2-decanone (755 mg, 4.38 mmol, jrr-b110-10) was added in one portion. Carbon tetrabromide (1.85 g, 5.58 mmol, Aldrich, 99%) was dissolved in distilled CH_2Cl_2 (10 mL) and was added (with stirring) to the chilled solution over 15 minutes to yield a clear, light brown solution. The solution was stirred at 0 °C under argon and in the dark. After 4 hours, TLC analysis (jrr-c014-2) indicated the consumption of the reagent alcohol.

At five hours total reaction time, ice cold, Barnsted-filtered water (20 mL) was added, and the mixture was allowed to warm to room temperature. The organic fraction was removed and the aqueous solution was washed with CH_2Cl_2 (3 × 20 mL). The combined organic fractions were dried over $MgSO_4$ and concentrated on a rotary evaporator to yield 4.43 g of a light brown oil that crystallized upon standing. This oil was dissolved in CH_2Cl_2 and EtOH (10 mL, 1:1) and purified (in dim light) using flash column chromatography (19:1 hexanes:EtOAc). Concentration on a rotary evaporator yielded 610 mg (61%) of a colorless oil. TLC (9:1 hexanes:EtOAc) R_f = 0.16 (DNP, UV, I_2); ^{1}H NMR (400 MHz, $CDCl_3$, jrr-c015-6) δ 3.410 (t, 2H, J = 7.6 Hz, Br**H**$_2$CH$_2$); 2.426 (t, 2H, J = 7.8 Hz, CH$_2$C**H**$_2$CO); 2.142 (s, 3H, CH$_2$COC**H**$_3$); 1.855 (q, 2H, 7.2 Hz, BrCH$_2$C**H**$_2$); 1.424 (m, 2H, C**H**$_2$CH$_2$CO); 1.35-1.25 (m, 6H); ^{13}C NMR (100 MHz, $CDCl_3$, jrr-c015-7) δ 209.2, 43.9, 34.1, 32.9, 30.0, 29.3, 29.2, 28.7, 28.2, 23.9.

10-iodo-2-decanone (jrr-d070). 10-Iodo-2-decanone was prepared according to the method of Millar and Underhill.[87] In dim light, 10-hydroxy-2-decanone (1.23 g, 7.14 mmol, jrr-b110-10) was dissolved using 25 mL freshly distilled CH_2Cl_2 in an argon-flushed round-bottom flask. The flask was chilled in ice water; imidazole (2.0 g, 29 mmol, Baker) and triphenylphosphine (3.75 g, 14.3 mmol, Aldrich, 99%) were then added. The solution was stirred under argon for 10 minutes, at which time I_2 (3.75 g, 14.8 mmol, Baker) was added in one portion. The clear solution became yellow, then brown. It was allowed to stir (in the dark) at 0 °C for 30 minutes and then for 2 hours at room temperature, at which time TLC analysis (jrr-d070-3) indicated the loss of reagent alcohol.

At this time, HCl (50 mL, 1 M) was added to the reaction mixture, which was stirred for 10 minutes. The mixture was transferred to a separatory funnel, and the organic fraction was separated and then washed with Barnsted-filtered water (75 mL). The aqueous layer was washed with an additional portion of CH_2Cl_2 (25 mL). The combined organic fractions were dried over $MgSO_4$ to yield a clear, bright red solution. Concentration on a rotary evaporator provided 7.0 g of dark red solids. These were dissolved in CH_2Cl_2 (~10 mL) and purified (in dim light) using flash column chromatography (19:1 hexanes:EtOAc). Concentration on a rotary evaporator (and standing, unsealed, overnight) yielded 1.25 g (62.2%) of a colorless oil. TLC (19:1 hexanes:EtOAc) R_f = 0.17 (UV, I_2); ^{1}H NMR (400 MHz, $CDCl_3$, jrr-d071-6) δ 3.190 (t, 2H, J = 7.2 Hz, $CH_2C\mathbf{H_2}I$), 2.424 (t, 2H, J = 7.6 Hz, $CO_2C\mathbf{H_2}CH_2$), 2.050 (s, 3H, $C\mathbf{H_3}CO_2$), 1.818 (q, 2H, J = 7.6 Hz, $C\mathbf{H_2}CH_2I$), 1.6-1.5 (m, 4H), 1.4-1.2 (m, 6H); ^{13}C NMR (50.3 MHz, $CDCl_3$ jrr-b120-7 – a different sample synthesized via the same method) δ 209.5, 44.0, 33.7, 30.7, 30.1, 29.4, 29.3, 28.6, 24.0, 7.5.

2,3,4,5-tetramethylpyrazine-*N*-oxide (jrr-a134). Impure material was provided by Julie Cooper (JAC-A-85-10). NMR analysis (jrr-a081-1) indicated a mixture of the monooxidized and (probably) dioxidized material. Dioxidized material was removed from the desired mono-*N*-oxide by sublimation at 0.05 torr and approximately 40 °C overnight. In this fashion, 4.70 g of the mixture provided 3.90 g of purified mono-*N*-oxide, including several diffraction-quality crystals (vials jrr-a137-7 and 8, box 403). ^{1}H NMR (400 MHz, $CDCl_3$, jrr-a134-3b) δ 2.518 (s, 6H), 2.465 (s, 6H).

2,3,4,5-tetramethylpyrazinium-*N*-oxide perchlorate, needle crystals (jrr-a136). A 10 mL reaction tube was flushed with a stream of dry nitrogen. Solid 2,3,4,5-tetramethylpyrazine-*N*-oxide (380 mg, 2.50 mmol, jrr-a134-3) was added to this tube, which was capped with a rubber septum fitted with an "open" needle that allowed a stream of argon gas to flow over the sample. This solid was dissolved in CH_3OH (500 μL, bubbled with nitrogen gas). An aqueous solution of perchloric acid (215 mL, 2.50 mmol, B&A, bubbled with nitrogen gas), was added slowly with vigorous evolution of heat. Storage overnight at –15° did not induce crystallization. The solution was warmed to room temperature and was concentrated (by aspiration) until solids were noted (to less than approximately one-half the original volume). Additional CH_3OH (100 μL) was added to dissolve the solids, and an "open" syringe needle was inserted into the septum. The solution was allowed to evaporate under a slow stream of nitrogen. Although the tube supplying nitrogen gas blew off, evaporation produced a thick solution with many crystals. The crystals were collected, dried on lens paper and stored in nitrogen-flushed vials (jrr-a141-3).

2,3,4,5-tetramethylpyrazinium-*N*-oxide perchlorate, prismatic and hexagonal plate crystals (jrr-a168). A 10 mL screw-top vial was flushed with a stream of dry argon. Solid 2,3,4,5-tetramethylpyrazine-*N*-oxide (395 mg, 2.60 mmol, jrr-a137-6) was added to this tube, which was capped with a rubber septum fitted with an "open" needle that allowed a stream of argon gas to flow over the sample. This material was dissolved using CH_3NO_2 (300 μL, bubbled with argon gas). An aqueous solution of perchloric acid (225 μL, 2.60 mmol, B&A, bubbled with argon gas) was added slowly with vigorous

evolution of heat. An "open" syringe needle was inserted into the septum and the solution was allowed to evaporate under a slow stream of argon. At the appearance of white solids (after 3 hours), the mixture was warmed in a 47 °C oil bath and redissolved with additional argon-flushed CH_3NO_2 (70 mL). The oil bath was allowed to cool slowly. After 70 minutes, crystals were noted at 41.5 °C; the solution was allowed to cool overnight to 22 °C, at which time 191 mg of prismatic (octahedral) crystals were collected on lens paper and stored in an argon-flushed vial (jrr-a168-7). The mother liquor was capped and allowed to evaporate under a slow stream of argon gas. A second batch of prismatic crystals was collected after seven days (jrr-a177-5). Upon standing two additional days (capped, under argon) a third crop of crystals was noted. This crop contained both prismatic blocks and thin hexagonal plates. These were washed out of the vial with THF, dried on lens paper, and stored in argon-flushed vials (jrr-a188-10).

2,3,4,5-tetramethylpyrazinium-*N*-oxide perfluoroborate (jrr-b280). A 10 mL reaction tube was flushed with a stream of dry argon. Solid 2,3,4,5-tetramethylpyrazine-*N*-oxide (250 mg, 1.64 mmol, jrr-a137-8) was added to this tube, which was capped with a rubber septum fitted with an "open" needle that allowed a stream of argon gas to flow over the sample. This material was dissolved using CH_3NO_2 (200 μL, bubbled with argon gas). The solution was gently warmed in a water bath to complete solvation and then allowed to cool. Crystallization was noted when the solution reached room temperature. A 50% aqueous solution of HBF_4 (210 μL, 1.64 mmol, Lancaster, bubbled with argon gas) was added, and the crystalline solids dissolved to yield a clear, colorless solution. The solution was allowed to evaporate under a slow stream of argon. After

twelve days a white, crystalline solid was noted. Repeated attempts at recrystallization from mixtures CH_3NO_2 and water were performed (jrr-c013), but no crystals were collected. It is believed that quality crystals may be obtained via methods like those utilized on jrr-c013.

1-methylcyclononanol (jrr-b022). 1-Methylcyclononanol was prepared according to a method adapted from Williamson.[82] A 50 mL round-bottom flask was flushed with argon; to it was added cyclononanone (500 mg, 3.57 mmol, Aldrich 95%) and freshly distilled Et_2O (10 mL). The flask was chilled in ice water under a stream of argon. A solution of methyl magnesium bromide (2.6 mL, 7.1 mmol, 3.0 M in Et_2O, Aldrich, 99.9%) and freshly distilled Et_2O (20 mL) was added to a dry, argon-flushed addition funnel. Over 45 minutes, this Grignard reagent was added to the rapidly stirred, ice cold cyclononanone solution. The evolution of gas and the formation of precipitate accompanied the addition. After 22 hours at 0 °C, HCl (15 mL, 1 M) was added quickly to the cold mixture. The mixture was then transferred to a larger flask using an additional 10 mL HCl (1 M) and was then allowed to warm slowly.

After four hours, the mixture was transferred to a separatory funnel and the organic fraction removed. The aqueous fraction was extracted with Et_2O (3 × 50 mL). The combined organic fractions were washed with Barnsted-filtered water and brine, and dried over $MgSO_4$ to yield a clear, colorless solution. TLC analysis (jrr-b023-4) suggested some impurity. The dried fraction was swirled with 3 g decolorizing carbon and allowed to stand for 30 minutes. The filtered solution was concentrated on a rotary evaporator and under high vacuum to yield 470 mg (84.4%) of a white, oily solid with a

characteristic, bitter odor. mp 41–43 °C (jrr-b030-8); TLC (4:1 hexanes:EtOAc) R_f = 0.35 (PAA); ^{1}H NMR (400 MHz, $CDCl_3$, jrr-b030-6) δ 1.8–1.4 (m, 16H); 1.165 (s, 3H, C**H**$_3$); ^{13}C NMR (50.3 MHz, $CDCl_3$, jrr-b030-6) δ 74.6, 35.7, 29.6, 27.5, 22.5, 20.3.

1,4-bis(*p*-toluenesulfonyloxy)butane (jrr-b128). This preparation follows the method of Earl and Harmon.[88] A dry, 50 mL round-bottom flask was flushed with argon. In this flask, 1,4-butanediol (225 μL, 2.51 mmol, Aldrich, 99+%) and *p*-toluenesulfonyl chloride (1.00 g, 5.27 mmol, Acros, 99+%) were dissolved in freshly distilled CH_2Cl_2 (5 mL). The solution was chilled in ice water and a solution of pyridine (5.1 mL, 63 mmol, Fisher, ACS reagent) and CH_2Cl_2 (5 mL) was added over a period of 30 minutes using an addition funnel. The clear, colorless solution was allowed to stir while cold under argon. After 1 hour, a white precipitate was noted.

After 2.5 hours the reaction mixture was filtered (unsuccessfully) on a Büchner funnel. The entire reaction mixtures was then recombined and transferred to a separatory funnel with CH_2Cl_2 and washed with HCl (two portions, 1 M), Barnsted-filtered water and brine, then dried over $MgCl_2$ to yield a clear, colorless organic fraction. Concentration on a rotary evaporator provided a heavy, colorless oil. This oil was dissolved into 15 mL hot EtOH and allowed to stand (lightly capped). After 3.5 hours, many white crystals (plates) had formed. The flask was chilled in ice water (for 10 minutes) and filtered. The filtered solids were washed with cold EtOH and dried in a vacuum desiccator to yield 570 mg (57.0%) of white, crystalline solids. mp 81–83 °C (jrr-b130-2); TLC (95:5 CH_2Cl_2:MeOH, plus a few drops of NH_4OH) R_f = 0.83 (I_2); ^{1}H NMR (400 MHz, $CDCl_3$, jrr-b130-5) δ 7.765 (d, 4H, protons ortho to sulfonyl group);

7.355 (d, 4H, protons meta to sulfonyl group); 3.990 (m, 4H, $ArSO_3C\mathbf{H}_2CH_2$); 2.460 (s, 6H, $ArC\mathbf{H}_3$); 1.701 (m, 4H, $ArSO_3CH_2CH_2$); ^{13}C NMR (50.3 MHz, $CDCl_3$) δ 145.2, 133.1, 130.2, 128.1, 69.6, 25.3, 21.9.

7.7 Copyright Permissions

Powered by RIGHTSLINK COPYRIGHT CLEARANCE CENTER, INC. Home | Account Info | Help

nature publishing group

Title: Stress-induced domain reorientation in urea inclusion compounds
Author: Michael E. Brown, Mark D. Hollingsworth
Publication: Nature
Publisher: Nature Publishing Group
Date: Jul 27, 1995
Copyright © 1995, Nature Publishing Group

Logged in as:
Jeremy Rush
LOGOUT

Order Completed

Thank you very much for your order.

This is a License Agreement between Jeremy R Rush ("You") and Nature Publishing Group ("Nature Publishing Group"). The license consists of your order details, the terms and conditions provided by Nature Publishing Group, and the payment terms and conditions.

Get the printable license.

Order Details | Billing & Contact Info

License Number	1847650466188
License date	Dec 14, 2007
Licensed content publisher	Nature Publishing Group
Licensed content publication	Nature
Licensed content title	Stress-induced domain reorientation in urea inclusion compounds
Licensed content author	Michael E. Brown, Mark D. Hollingsworth
Volume number	
Issue number	
Pages	
Year of publication	1995
Portion used	Full paper
Requestor type	Student
Type of Use	Thesis / Dissertation
PO Number	
Total	$0.00

ORDER MORE... CLOSE WINDOW

Science
AAAS

Permissions Letter

Ref # 07-24476

DATE: Friday, December 14, 2007

TO: Jeremy Rush
Kansas State University
916 Glenhaven Circle
Liberty, MO 64068

FROM: Elizabeth Sandler, Rights and Permissions
RE: Your request for permission dated 12/14/07

Regarding your request, we are pleased to grant you non-exclusive, non-transferable permission to use the AAAS material identified below in your dissertation or thesis identified below, but limited to the formats identified below, and provided that you meet the conditions / requirements below. Such permission is for one time use and therefore does not include permission for future editions, revisions, additional printings, updates, ancillaries, other formats, translations, or promotional pieces, unless otherwise permitted below. This permission does not apply to figures / artwork that are credited to non-AAAS sources. This permission does not include the right to modify AAAS material.

The following credit line must be printed along with the AAAS material: "From [Insert Full Reference Citation]. Reprinted with permission from AAAS."

This permission covers the use of the AAAS material identified herein in the following format versions of your dissertation/thesis:
[x] print
[x] microform
[x] Digitized / electronic versions , provided the reprinted AAAS material remains in situ and is not made digitally available separated from your dissertation/thesis

AAAS agrees that ProQuest/UMI may supply copies of the dissertation/thesis on demand.

If the requested material is sourced to or references non-AAAS sources, you must obtain authorization from that source as well.

Permission fees are waived in this instance. AAAS reserves the right to charge for reproduction of AAAS controlled material in the future.

AAAS must publish the full paper prior to use of any text.

AAAS does not supply photos or artwork. Use of the AAAS material must not imply any endorsement by the American Association for the Advancement of Science. This permission is not valid for the use of the AAAS and/or SCIENCE logos.

Permission is valid for use of the following AAAS material only:
Fig 1a, b & 5 from Hollingsworth et al., SCIENCE 273:1355 (1996)
In the following work only:
CRYSTAL GROWTH, GUEST ORDERING AND FERROELASTIC PROPERTIES OF UREA INCLUSION COMPOUNDS published by KSU in 2007

Thank you for writing. If you have any questions please call me at (202) 326-6765 or write to me via fax at (202) 682-0816. For international calls, +1 is the country code for the United States.

Headquarters:
1200 New York Avenue, NW, Washington, D.C. 20005 USA

RE: McBride, J. M., *Adv. Mater., (1989), 1, 87-89.*
Permission obtained December 16, 2007.

Dear Customer,

Thank you for your email.

We hereby grant permission for the requested use expected that due credit is given to the original source.
Please note that the author's permission is also required.

If material appears within our work with credit to another source, authorisation from that source must be obtained.

Credit must include the following components:
- Books: Author(s)/ Editor(s) Name(s): Title of the Book. Page(s). Publication year. Copyright Wiley-VCH Verlag GmbH & Co. KGaA. Reproduced with permission.

- Journals: Author(s) Name(s): Title of the Article. Name of the Journal. Publication year. Volume. Page(s). Copyright Wiley-VCH Verlag GmbH & Co. KGaA. Reproduced with permission.

With kind regards

Bettina Loycke
****

Bettina Loycke
Copyright & Licensing Manager
Wiley-VCH Verlag GmbH & Co. KGaA
Boschstr. 12
69469 Weinheim
Germany

Phone: +49 (0) 62 01- 606 - 280
Fax: +49 (0) 62 01 - 606 - 332
Email: rights@wiley-vch.de

Wiley Bicentennial: Knowledge for Generations
1807-2007

References Cited

1. Hollingsworth, M. D. Personal communication to J. R. Rush (2002).
2. Brown, M. E., Chaney, J. D., Santarsiero, B. D. & Hollingsworth, M. D. Superstructure topologies and host-guest interactions in commensurate inclusion compounds of urea with bis(methyl ketone)s. *Chem. Mater.* **8**, 1588-1591 (1996).
3. Hollingsworth, M. D., Werner-Zwanziger, U., Brown, M. E., Chaney, J. D., Huffman, J. C., Harris, K. D. M. & Smart, S. P. Spring-loading at the molecular level. Relaxation of guest-induced strain in channel inclusion compounds. *J. Am. Chem. Soc.* **121**, 9732-9733 (1999).
4. Aliev, A. E., Smart, S. P., Shannon, I. J. & Harris, K. D. M. Structural and dynamic properties of the 1,10-dibromodecane/urea inclusion compound, investigated by variable-temperature powder X-ray diffraction, solid-state ^{2}H NMR lineshape analysis and solid-state ^{2}H NMR spin-lattice relaxation time measurements. *J. Chem. Soc., Faraday Trans.* **92**, 2179-2185 (1996).
5. Harris, K. D. M., Smart, S. P. & Hollingsworth, M. D. Structural properties of α,ω–dibromoalkane/urea inclusion compounds: A new type of interchannel guest molecule ordering. *J. Chem. Soc., Faraday Trans.* **87**, 3423-3429 (1991).
6. Smart, S. P., El Baghadadi, A., Guillaume, F. & Harris, K. D. M. Conformational and vibrational properties of α,ω–dihalogenoalkane/urea inclusion compounds: A Raman scattering investigation. *J. Chem. Soc., Faraday Trans.* **90**, 1313-1322 (1994).
7. Hollingsworth, M. D., Brown, M. E., Hillier, A. C., Santarsiero, B. D. & Chaney, J. D. Superstructure control in the crystal growth and ordering of urea inclusion compounds. *Science (Washington, D. C.)* **273**, 1355-1359 (1996).
8. Peterson, M. L. & Hollingsworth, M. D. X-ray crystal structure solution mp101. (2001).
9. Gavezzotti, A. Packing analysis of organic crystals containing C=O or CN groups. *J. Phys. Chem.* **94**, 4319-4325 (1990).
10. Harris, K. D. M. & Thomas, J. M. Structural aspects of urea inclusion compounds and their investigation by X-ray diffraction: A general discussion. *J. Chem. Soc., Faraday Trans.* **86**, 2985-96 (1990).
11. Hollingsworth, M. D. Personal communication to J. R. Rush (2005).
12. Hollingsworth, M. D. & Harris, K. D. M. "Urea, thiourea, and selenourea" in *Comprehensive Supramolecular Chemistry*, vol. 6 (eds. MacNicol, D. D., Toda, F. & Bishop, R.) (Pergamon Press, New York, 1996) pp. 177-237.
13. Rush, J. R. Laboratory notebook entry jrr-a018-5. (2002).
14. Rush, J. R. Laboratory notebook entry jrr-b053. (2003).
15. Rush, J. R. Laboratory notebook entry jrr-b170. (2003).
16. Rush, J. R. Laboratory notebook entry jrr-b164 and b165. (2003).
17. Rush, J. R. Laboratory notebook entry jrr-b176-12. (2003).
18. Rush, J. R. Laboratory notebook entry jrr-b176-8. Filename jr0316\work\ortho\jr0316m._ls. (2003).
19. Rush, J. R. Laboratory notebook entry jrr-e264. Filename e264.prp. X-ray data set jr0316. (2005).

20. Rush, J. R. Laboratory notebook entry jrr-e264. X-ray data set jr0316. (2005).
21. Rush, J. R. Laboratory notebook entry jrr-e264-5. X-ray data set jr0316; filename jrr-e264-5.res. (2005).
22. Geiger, T. A. M.S. Thesis, Kansas State University. (2006).
23. Rabiller, P. Improc, a program executable under MATLAB.
24. Guinier, A. *X-Ray Diffraction In Crystals, Imperfect Crystals and Amorphous Bodies*, (Dover Publications, Inc., New York, 1994), pp. 309-314.
25. Rush, J. R. Laboratory notebook entry jrr-b156. (2003).
26. Rush, J. R. Laboratory notebook entry jrr-b142-6. (2003).
27. Schlenk, W., Jr. Asymmetric urea inclusion lattice. IV. Absolute configuration of the lattice. *Liebigs Ann. Chem.* **7**, 1195-1209, (1973). This work was discussed by Hollingsworth, M. D. & Harris, K. D. M. "Urea, thiourea, and selenourea" in *Comprehensive Supramolecular Chemistry*, vol. 6 (eds. MacNicol, D. D., Toda, F. & Bishop, R.) (Pergamon Press, New York, 1996) pp. 177-237.
28. Chickos, J. S., Bausch, M. & Alul, R. Stereospecific synthesis of optically active succinic-d_2 acid. *J. Org. Chem.* **46**, 3559-3562 (1981).
29. Clark, A., Rush, J. R. & Hollingsworth, M. D. *Unpublished Observation* (2003).
30. Carey, F. A. & Sundberg, R. J. *Advanced Organic Chemistry, Part A: Structure and Mechanisms*, (Kluwer Academic/Plenum Publishers, Boston, 2000), pp. 295-298.
31. Rush, J. R. & Clark, A. H. Laboratory notebook entry jrr-b128. (2003).
32. Brown, C. A. Facile reaction of potassium hydride with ketones. *J. Org. Chem.* **39**, 1324-1325 (1974).
33. Rush, J. R. Laboratory notebook entry jrr-b161. (2003).
34. Stork, G. & Landesman, H. K. A new alkylation of carbonyl compounds. II. *J. Am. Chem. Soc.* **78**, 5128-5129 (1956).
35. Stork, G., Brizzolara, A., Landesman, H., Szmuszkovicz, J. & Terrell, R. The enamine alkylation and acylation of carbonyl compounds. *J. Am. Chem. Soc.* **85**, 207-222 (1963).
36. White, W. A. & Weingarten, H. A versatile new enamine synthesis. *J. Org. Chem.* **32**, 213-214 (1967).
37. Heyl, F. W. & Herr, M. E. "Enamine" derviatives of steroidal carbonyl compounds. II. *J. Am. Chem. Soc.* **75**, 1918-1920 (1953).
38. Holland, J., M., Lewis, M. & Nelson, A. Desymmetrization of a centrosymmetric diepoxide: Efficient synthesis of a key intermediate in a total synthesis of hemibrevetoxin B. *J. Org. Chem.* **68**, 747-753 (2003).
39. DeVilbiss, D. & Riordan, E. *Unpublished Results, Chemistry 551 (Mark D. Hollingsworth and Jeremy R. Rush, instructors)* (2003).
40. Carlson, R., Phan-Tau-Lin, R., Mathieu, D., Ahouande, F. S., Babadjamain, A. & Metzger, J. Optimal synthesis of enamines from methyl ketones. A comparative study of two different synthetic methods. *Acta Chemica. Scand. B* **32**, 335-342 (1978).
41. Carlson, R., Nilsson, Å. & Strömqvist, M. Optimum conditions for enamine synthesis by an improved titanium chloride procedure. *Acta Chemica. Scand. B* **37**, 7-13 (1983).

42. Carlson, R. & Nilsson, Å. Improved titanium tetrachloride procedure for enamine synthesis II. Scope of the reaction. *Acta Chemica. Scand. B* **38**, 49-53 (1984).
43. Buerger, M. J. *Crystal-Structure Analysis*, (Robert E. Krieger Publishing Company, Huntington, New York, 1980), pp. 509-521.
44. Rush, J. R. Laboratory notebook entry jrr-a029. (2002).
45. Dewar, M. J. S., Zoebisch, E. G., Healy, E. F. & Stewart, J. J. P. Development and use of quantum mechanical molecular models. 76. AM1: A new general purpose quantum mechanical molecular model. *J. Am. Chem. Soc.* **107**, 3902-3909, (1985). Included in the Chem3D Pro software package, v. 3.5.1. CambridgeSoft Corporation (1997).
46. Bondi, A. van der Waals volumes and radii. *J. Phys. Chem.* **68**, 441-451 (1964).
47. Rush, J. R. Laboratory notebook entry jrr-a033-3b. (2002).
48. Rush, J. R. Laboratory notebook entry jrr-a056-35. (2002).
49. Rush, J. R. Laboratory notebook entry jrr-a026. (2002).
50. Rush, J. R. Laboratory notebook entry jrr-a053-12. (2002).
51. Desper, J. M. & Rush, J. R. Laboratory notebook entry jrr-f011-1. X-ray data set jr0201. (2002).
52. Rush, J. R. Laboratory notebook entry jrr-f011-3. X-ray data set jr0201. (2005).
53. Rush, J. R. Laboratory notebook entry jrr-f011-3. X-ray data set jr0201; filename jr0201m.prp. (2005).
54. Rush, J. R. Laboratory notebook entry jrr-f012. (2005).
55. Flack, H. D. On enantiomorph-polarity estimation. *Acta Crystallogr. A* **39**, 876-881 (1983).
56. Rush, J. R. Laboratory notebook entry jrr-f012-13. X-ray data set jr0201. (2005).
57. Rush, J. R. Laboratory notebook entry jrr-f012-14. X-ray data set jr0201. (2005).
58. Rush, J. R. Laboratory notebook entry: jrr-f154. (2006).
59. Rush, J. R. Laboratory notebook entry jrr-f012-11. X-ray data set jr0201; filename f012-11.ins. (2005).
60. Rush, J. R. Laboratory notebook entry jrr-f251-1. (2007).
61. Rush, J. R. Laboratory notebook entry jrr-f251-3. (2007).
62. Ladd, M. & Palmer, R. *Structure Determination by X-ray Crystallography*, (Kluwer Academic/Plenum Publishers, New York, 2003), p. 167.
63. SAINT v. 6.36A. *Bruker Analytical X-ray Systems* (1998).
64. Skoog, D. A., Holler, F. J. & Nieman, T. A. *Principles of Instrumental Analysis*, (Saunders College Publishing, Philadelphia, 1998), pp. 99-100.
65. Allen, F. H., Kennard, O., Watson, D. G., Bremmer, L., Orpen, G. & Taylor, R. Tables of bond lengths determined by X-ray and neutron diffraction. Part 1. Bond lengths in organic compounds. *J. Chem. Soc. Perk. Trans. 2*, S1-S19 (1987).
66. Champion, B. & Hollingsworth, M. D. *Unpublished Observation* (2001).
67. Rush, J. R. Laboratory notebook entry jrr-b026. (2003).
68. Gordon, A. J. & Ford, R. A. *The Chemist's Companion: A Handbook of Practical Data, Techniques, and References*, (John Wiley and Sons, Inc., New York, 1972), pp. 429-436.

69. Still, W. C., Kahn, M. & Mitra, A. Rapid chromatographic technique for preparative separations with moderate resolution. *J. Org. Chem.* **43**, 2923-2925 (1978).
70. Pyris v. 2.0.4.0. *The Perkin-Elmer Corporation* (1997).
71. *CRC Handbook of Chemistry and Physics, 50th edition*, (ed. Weast, R. C.) (The Chemical Rubber Company, Cleveland, 1969) p. C-264.
72. Angott, A. Laboratory notebook entry AMA-A-29. (2003).
73. Nikon. Microscopy U. http://www.microscopyu.com/sitemap.html, (2000–2006).
74. Drude, P. *The Theory of Optics*, (Dover Publications, Inc., New York, 1959), pp. 84-86 and 91-92.
75. Glazer, A. M., Lewis, J. G. & Kaminsky, W. An automatic optical imaging system for birefringent media. *Proc. Roy. Soc. Ser. A* **452**, 2751-2765 (1996).
76. Gay, P. *An Introduction to Crystal Optics*, (Longmans, Green and Co., Ltd., London, 1967), pp. 120-124.
77. Geday, M. A., Kaminsky, W., Lewis, J. G. & Glazer, A. M. Images of absolute retardance $L \bullet \Delta n$, using the rotating polarizer method. *J. Microsc.* **198**, 1-9 (2000).
78. Burkhardt, E., Ye, Z. G. & Schmid, H. Low and high tempeature uniaxial stress devices for the study of ferroelastic crystals. *Rev. Sci. Instrum.* **66**, 3888-3893 (1995).
79. Brown, M. E. & Hollingsworth, M. D. Stress-induced domain reorientation in urea inclusion compounds. *Nature (London)* **376**, 323-7 (1995).
80. Black, A. A. & Abel, M. J. Laboratory notebook entry mja-a-14. (2002).
81. Rush, J. R. Laboratory notebook entry jrr-f202. (2006).
82. Williamson, K. L. "Grignard synthesis of triphenylmethanol and benzoic acid" in *Macroscale and Microscale Organic Experiments, second edition*, (D. C. Heath and Company, Toronto, 1994) pp. 364-378.
83. Zhang, W.-C. & Li, C.-J. A direct retro-Barbier fragmentation. *J. Org. Chem.* **65**, 5831-5833 (2000).
84. Peppe, C., Lang, E. S., Ledesma, G. N., de Castro, L. B., do Rego Barros, O. S. & Mello, P. d. A. Indium(I) bromide-mediated regioselective markovnikov hydroselenation, diselenation and hydration of terminal alkynes with diphenyldiselenide in aqueous media. *Synlett*, 3091-3094 (2005).
85. Brown, M. E. Laboratory notebook entry MEB-F-44.
86. Geiger, T. A. Masters Thesis, Kansas State University. (2006).
87. Millar, J. G. & Underhill, E. W. Synthesis of chiral bis-homoallylic epoxides. A new class of lepidopteran sex attractants. *J. Org. Chem.* **51**, 4726–4728 (1986).
88. Earl, R. A. & Harmon, R. E. Carcinostatic sulfonic acid esters of butyne- and butane-1,4-diols. *J. Med. Chem.* **9**, 776-778 (1966).